NACA RM E56D06

NACA

RESEARCH MEMORANDUM

EXPERIMENTAL INVESTIGATION OF A TRANSONIC COMPRESSOR

ROTOR WITH A 1.5-INCH CHORD LENGTH AND

AN ASPECT RATIO OF 3.0

III – BLADE-ELEMENT AND OVER-ALL PERFORMANCE AT

THREE SOLIDITY LEVELS

By Edward R. Tysl and Francis C. Schwenk

Lewis Flight Propulsion Laboratory
Cleveland, Ohio

NATIONAL ADVISORY COMMITTEE
FOR AERONAUTICS
WASHINGTON
August 17, 1956

NACA RM E56D06

NASA Technical Library

3 1176 01435 8411

NATIONAL ADVISORY COMMITTEE FOR AERONAUTICS

RESEARCH MEMORANDUM

EXPERIMENTAL INVESTIGATION OF A TRANSONIC COMPRESSOR ROTOR

WITH A 1.5-INCH CHORD LENGTH AND AN ASPECT RATIO OF 3.0

III - BLADE-ELEMENT AND OVER-ALL PERFORMANCE AT

THREE SOLIDITY LEVELS

By Edward R. Tysl and Francis C. Schwenk

SUMMARY

Two low-solidity configurations of a 1.5-inch-chord transonic compressor rotor were tested to provide data on the effects of solidity on over-all and blade-element performance. These rotors were tested over a range of weight flows at speeds up to the corrected design tip speed of 1000 feet per second. The two low-solidity rotors consisted of 28 and 22 blades of the original 35-blade rotor and had tip solidities of 0.76 and 0.60, respectively. The original 35-blade rotor had a tip solidity of 0.95.

Comparison of relative total-pressure-loss coefficients for the hub and mean blade-element sections indicated no definite effect of solidity. Losses at the tip section also indicated no solidity effect at the lower speeds. At 90 and 100 percent of design speed, however, relative total-pressure-loss coefficient increased with decreasing solidity, contrary to available cascade data. Blade suction-surface Mach numbers seem to explain the increase in losses.

Deviation angles at minimum-loss incidence angles for the three rotors were nearly constant over the speed range tested. In addition, they agreed within 2° with values computed from Carter's rule.

Studies made with hot-wire anemometers on stall characteristics of the two low-solidity rotors indicated only nonperiodic flow fluctuations as weight flow was reduced at speeds of 50, 60, and 80 percent of design. Periodic rotating stall was observed in the high-solidity rotor at these speeds.

INTRODUCTION

Recent test results (ref. 1) of a transonic compressor rotor show some important effects of solidity (chord-to-spacing ratio) on the performance of such a blade row. A rather large increase in the minimum-loss level for a blade element close to the rotor tip was observed as solidity decreased. This phenomenon occurred at high inlet relative Mach numbers, and the change in loss level with solidity was not related to changes in blade loading as given by the diffusion factor, axial velocity ratio, or inlet relative Mach number with solidity.

In order to study solidity effects further and to substantiate the trends observed in reference 1, another transonic compressor rotor was tested with three solidity levels at the NACA Lewis laboratory. The rotor blades used in the investigation were the double-circular-arc blades of the compressor discussed in references 2 and 3, which describe the design, over-all-performance, and blade-element characteristics of a 35-blade, 1.5-inch-chord compressor rotor having a tip solidity of 0.95. Tip solidities of 0.76 and 0.60 were obtained by installing 28 and 22 blades in two new rotor disks at setting angles equal to the setting angles of the 35-blade rotor.

Certain similarities exist between these rotor blades and the rotor blades of reference 1. Both blades have double-circular-arc blade elements of about the same maximum-thickness-to-chord ratio. Blade-inlet angles are about equivalent. The major differences are the chord length and the tip-section camber angles. Tip-section (located approximately 10 percent of the passage height away from the outer wall) chord length and camber angle of the rotors of reference 1 were 2.25 inches and 13.8°, respectively. The tip-section camber angle of the 1.5-inch-chord rotors used in the present solidity tests was 6°.

The characteristics of 35-, 28-, and 22-blade rotors were determined for a range of weight flows at corrected tip speeds from 60 to 100 percent of design speed ($U_t/\sqrt{\theta}$ = 1000 ft/sec). Complete blade-element and over-all performance characteristics of the 28- and 22-blade rotors are presented in this report. References 2 and 3 give similar data for the 35-blade rotor. The blade-element characteristics of the 35-, 28-, and 22-blade rotors are compared herein.

SYMBOLS

Figure 1, which illustrates air angles, blade angles, and velocities, can be used to define these parameters more completely:

A_F compressor frontal area based on rotor tip diameter, 1.767 sq ft

c_p specific heat of air at constant pressure, Btu/(lb)(°R)

D   diffusion factor (ref. 7)

g acceleration due to gravity, 32.17 ft/sec^2

H   total enthalpy, $c_p g J T$, sq ft/sec^2

i incidence angle, angle between inlet relative air velocity vector and tangent to blade mean camber line at leading edge, deg

J   mechanical equivalent of heat, 778.2 ft-lb/Btu

M   Mach number

m_c factor in deviation-angle relation, function of blade angle

P   total pressure, lb/sq ft

r radius measured from axis of rotation, in.

T   total temperature, °R

U   blade speed, ft/sec

V   air velocity, ft/sec

w weight flow of air, lb/sec

β air angle, angle between air velocity and axial direction, deg

δ ratio of inlet total pressure to NACA standard sea-level pressure of 2116 lb/sq ft

δ^o deviation angle, angle between outlet relative air velocity vector and tangent to blade mean camber line at trailing edge, deg

η_{ad} adiabatic temperature-rise efficiency

θ ratio of inlet total temperature to NACA standard sea-level temperature of 518.7° R

κ blade angle, angle between tangent to blade mean camber line and axial direction, deg

σ solidity, ratio of blade chord measured along streamline to average blade spacing

φ   blade camber angle, difference between angles of tangents to mean
         camber line at leading and trailing edges, deg

$\bar{\omega}$ relative total-pressure-loss coefficient (ref. 4)

Subscripts:

b   blade element

m   mean radius

s   suction surface

t   tip of rotor

z   axial direction

θ   tangential direction

1   depression tank

2   upstream of rotor, location of inlet static-pressure rake

3   rotor inlet

4   rotor outlet

Superscript:

'   denotes conditions relative to blade row

APPARATUS AND PROCEDURE

With the exception of the number of blades, the two low-solidity
rotors used in this investigation are exact replicas of the 1.5-inch-
chord transonic compressor rotor of references 2 and 3. Therefore,
blade-setting angles and blade-inlet and -outlet angles are identical.
Values of solidity along with values of blade-inlet and -outlet angles
at several radii are given in table I for the three rotor configurations.

The instrumentation, test procedures, and calculations used with
each rotor are similar and are described in references 2 and 3. These
references also describe the compressor test rig (fig. 2) in which the
rotors were tested.

The rotors were operated over a range of weight flow at corrected
tip speeds of 60, 70, 80, 90, and 100 percent of design corrected tip

speed (1000 ft/sec). The performance of each rotor is analyzed by the blade-element approach described in references 1 and 4.

OVER-ALL PERFORMANCE

Weight Flow, Pressure Ratio, and Efficiency

The over-all performance of the three configurations of the 1.5-inch-chord transonic compressor rotor is presented in figure 3. Mass-averaged total-pressure ratio and mass-averaged adiabatic efficiency are plotted against corrected weight flow per unit frontal area. Data for speeds of 60, 70, 80, 90, and 100 percent of design speed are presented for a weight-flow range at each speed.

Maximum weight flow increases as solidity decreases for all speeds except design speed. At design speed, maximum weight flow remains essentially constant as solidity decreases. The 35-blade rotor choked at maximum weight flow at design speed, as shown by the data of figure 3(a). The efficiency and total-pressure-ratio variations with weight flow for the rotor approach a vertical line at the maximum flow and, thus, indicate rotor choking. The maximum weight flows at design speed for the two lower-solidity rotors, however, seem to be limited by choking in the piping system used in this investigation.

The minimum weight flow at each speed was arbitrarily limited by rotor blade vibrations detected with a magnetic pickup located in the outer casing. Blade vibrations were assumed to indicate the start of stalled or unstable operation of the compressor. No definite effect of solidity on minimum weight flow was found except at design speed. At design speed, lower flow rates were reached at higher solidities.

With the exception of the operating conditions near maximum weight flow, the average total-pressure-ratio level varies directly with solidity at each speed. Small differences in total-pressure-ratio levels are found at the lower speeds, and large differences at design speed. This is due to the combination of work-coefficient and loss-coefficient variations with solidity. This combination is also responsible for the variation of adiabatic efficiency, which is similar to the total-pressure-ratio variation. The peak-efficiency operating point for each solidity occurs near maximum weight flow at speeds below design.

At 60- and 70-percent design speed, peak-efficiency values for the three rotors are approximately equal. At 80-percent speed, the peak efficiency for the two higher-solidity rotors are alike but lower than the peak efficiency obtained by the 22-blade rotor. At 90-percent speed, however, the efficiency of the low-solidity rotor drops below that of the other two rotors, which are still about equal. At design speed, peak

efficiency varies directly as solidity (the lower the solidity, the lower the peak efficiency) and occurs near the middle of the weight-flow range.

Stall Characteristics

The rotating-stall characteristics of the 28- and 22-blade versions of the 1.5-inch-chord transonic compressor rotor were investigated as in the tests of the 35-blade rotor (ref. 2). Hot-wire anemometers were located downstream of the rotors to detect flow fluctuations at 50, 60, and 80 percent of design speed.

At speeds of 50 and 60 percent of design, the 35-blade rotor first operated with two full-span stall zones at a weight flow lower than the peak-pressure-ratio operating condition (fig. 3). As weight flow was reduced further, the rotor operated with only one full-span zone. At 80-percent design speed, only one full-span rotating-stall zone was observed at reduced weight flows.

No periodic stalls were observed for the low-solidity (28- and 22-blade) rotors at low weight flows. At high weight flows, only blade wakes were detected by the hot-wire anemometers. As weight flow was reduced, blade wakes were gradually replaced by random flow fluctuations. The amplitude of the flow fluctuations or random stalls increased as weight flow decreased. Similar stall characteristics are reported in reference 1.

RADIAL VARIATIONS

Rotor-Inlet Conditions

Rotor-inlet data for the three solidities are given in figure 4 to indicate possible effects of changes of solidity and rotor performance on the inlet velocity profile. Figure 4 shows the radial variations of inlet absolute Mach number represented by the ratio of Mach number to mean-radius Mach number. Variations of Mach number shown in the figure are for 80- and 100-percent design speed and for a range of weight flows at each speed. Since there were no inlet guide vanes, the inlet tangential velocity component was assumed zero. The radial static-pressure variation for rotor-inlet calculations (station 3) was faired between the readings from outer- and inner-wall static taps with a trend similar to that recorded from the inlet static-pressure rake (station 2). This procedure was considered justifiable because of the small area change and small static-pressure change between stations 2 and 3 (fig. 1).

The design variation of inlet absolute Mach number was determined from previous investigations which used the same inlet configuration.

Figure 4 shows that (except for the tip region) the inlet Mach number profiles for the three rotors compare very well with the design variation. At 80 percent of design speed (fig. 4(b)), no effect of solidity on the inlet Mach number profile is shown. However, at design speed (fig. 4(a)) slight changes in the inlet Mach number profile occurred in the tip region as the solidity was varied. This observation indicates a change in the flow about the tip region at the high speed level.

Total-Pressure Ratio, Work Coefficient, and Efficiency

Data for the three solidities at nearly equal weight flows and good operating conditions are presented in figure 5 for speeds of 80 and 100 percent of design speed at the rotor outlet. The radial variations of blade-element adiabatic efficiency $\eta_{ad,b}$, total-pressure ratio $(P_4/P_1)_b$, and work coefficient $(\Delta H/U_t^2)_b$ (nondimensional temperature rise) are shown.

At design speed (fig. 5(a)), the data represent conditions close to peak-efficiency operation for each of the rotors. From about the mean section on out toward the tip, pressure ratio increases as solidity increases. This increase in pressure ratio can be traced to (1) the increase in work coefficient and (2) the decrease in losses as solidity increases, which will be discussed later. These factors also result in increased efficiency with increase in solidity.

At 80-percent design speed, rotor-outlet conditions for the three solidities are shown for two weight flows (figs. 5(b) and (c)). At the higher weight flow (near peak-efficiency operation, fig. 5(b)), the radial outlet conditions for the three solidities are almost identical, with the exception of the tip-region performance of the 35-blade rotor. This drop in performance for the high solidity is probably due to choking. In order to obtain a better picture of the performance at this speed, outlet conditions at a reduced weight flow are presented in figure 5(c). The trends exhibited by each rotor are similar. In figure 5(c), the total-pressure ratio, work coefficient, and efficiency increase with increasing solidity.

BLADE-ELEMENT PERFORMANCE OF 28- AND 22-BLADE ROTORS

The blade-element characteristics for the 28- and 22-blade rotors are presented in figures 6 and 7, respectively, for three blade elements and for corrected rotor tip speeds of 60, 70, 80, 90, and 100 percent of design. The three blade elements, which are located 84, 50, and 10 percent of the passage height from the outer wall, are called hub, mean, and tip. The blade-element performance of the 35-blade rotor, as well as a definition of the blade elements, is reported in reference 3.

The blade-element characteristics plotted against incidence angle in figures 6 and 7 are: relative total-pressure-loss coefficient $\bar{\omega}'$, deviation angle δ^o, inlet relative Mach number M_3', axial velocity ratio $V_{z,4}/V_{z,3}$, blade-element loading represented by the diffusion factor D, work coefficient (nondimensional temperature rise) $\Delta H/U_t^2$, and blade-element adiabatic efficiency η_{ad}. These parameters are described in references 4 and 5. Construction of velocity diagrams is possible by means of these parameters. Velocity-diagram notations for a blade element are presented in figure 1.

The blade-element performance of the 28- and 22-blade rotors is very similar to that of the 35-blade rotor (ref. 3) and other transonic compressor rotors. For this reason, these figures are not discussed in detail in this report, but the data are largely used for solidity comparisons.

COMPARISON OF BLADE-ELEMENT PERFORMANCE FOR THREE SOLIDITY LEVELS

Blade-Element Losses

In order to compare blade-element losses of the 35-, 28-, and 22-blade rotors, variations of relative total-pressure-loss coefficient with incidence angle for the three rotors are presented in figure 8 at three blade-element sections for 60, 80, 90, and 100 percent of design speed. The blade-element sections at the hub, mean, and tip are located 84, 50, and 10 percent of the passage height from the outer wall, respectively. The losses for the hub and mean sections are considered first because of their general similarity to cascade results.

Hub- and mean-section losses. - The loss variations with incidence angle for the hub and mean sections are shown in figures 8(a) and (b), respectively. The loss variations with incidence angle for each rotor are similar at all speeds and agree with past rotor results and cascade data. At low speeds (low Mach numbers) there is a wide incidence-angle range for low-loss operation. At high speeds, this low-loss incidence-angle range is reduced, particularly at the low incidence angles. This is typical of cascade data and previously reported rotor results (refs. 4 and 6).

With respect to the level of minimum loss coefficient, low-speed two-dimensional-cascade data show a linear increase in loss coefficient with increasing solidity (ref. 7). For the low losses usually found at the hub and mean sections, the change in loss level with solidity is expected to be small and probably within experimental accuracy.

Hub-section losses (fig. 8(a)) at speeds below 90-percent design are relatively low, and there is no measurable variation in the loss level

with solidity. At design speed for the hub section and at 90 and 100 percent of design speed for the mean section, some variations in loss-coefficient level with solidity were observed; however, no definite trend can be established from these data.

Tip-section losses. - Figure 8(c) presents the tip-section variation of loss with incidence angle for the three solidities. Data at 60 percent of design speed show little solidity effect of any kind. The data at 80, 90, and 100 percent of design speed show a tendency for the minimum-loss incidence angle to decrease with decreasing solidity. However, at design speed, the minimum-loss incidence angles are not defined for the two low-solidity rotors, since it appears that the tip section was not operated at the lowest incidence angle possible. The cause is the rig choking discussed earlier.

Minimum-loss levels at 60- and 80-percent design speed are not affected by solidity. At 90-percent design speed, the two higher solid-ities have about the same minimum losses; however, losses for the low solidity are greater. At design speed, there is a definite effect of solidity on losses; losses increase as solidity decreases. Similar loss trends were observed in the solidity investigation of reference 1, with comparable values of solidity and rotational speeds.

The increase in loss as solidity is decreased is contrary to the trends shown by low-speed-cascade results (ref. 8). In order to find a reason for this contradiction of cascade results, several flow parameters (inlet relative Mach number, diffusion factor, and axial velocity ratio) on which losses may depend were investigated. Inlet relative Mach numbers at a given incidence angle and wheel speed do not vary with solidity, because the blade angles are equal in all three rotors.

Variations of diffusion factor D (a blade-loading parameter, ref. 7) and axial velocity ratio $V_{z,4}/V_{z,3}$ with incidence angle are shown in figure 9. This figure presents tip-section data for three solidity levels at design corrected tip speed (1000 ft/sec).

Diffusion factors for the three solidity levels are nearly equal; therefore, this parameter does not explain the observed loss variation with solidity. Although the diffusion-factor equation

$$D = 1 - \frac{V_2'}{V_1'} + \frac{V_{\theta,1}' - V_{\theta,2}'}{2\sigma V_1'} \tag{1}$$

contains solidity explicitly, implicit variations of other terms in the equation with solidity cause the diffusion factor to remain nearly constant over the range of solidities tested.

Tip-section axial velocity ratio is higher for the lowest solidity than for the other two solidities. If axial velocity ratio had any effect at all, an increase would reduce losses; therefore, the axial velocity ratio does not account for an increase in losses with a decrease in solidity.

In order to compare tip-section loss levels at design corrected tip speed with past results, loss coefficients in the region of minimum loss taken from faired values of figures 6(c) and 7(c) are plotted in figure 10 against corresponding faired values of diffusion factor D. Also shown in figure 10 are tip-section data from the solidity investigation of reference 1 for a corrected tip speed of 1000 feet per second and the band or range of losses for a number of rotor tip sections as compiled in reference 7.

Trends exhibited by the rotors of this investigation and of reference 1 in figure 10 are similar in that only data from the highest solidity of each investigation fall within the band of previous results (ref. 7). The data for the lower solidities fall above the band, the lowest-solidity data being farther away.

Figure 10 also shows that for equal solidities the tip-section losses of the rotor of reference 1 are higher than the losses observed in the present investigation. At the highest-solidity level ($\sigma_t \approx 1.0$), the difference in loss level can be accounted for by the difference in the diffusion factor. However, for low solidity, changes in blade loading as measured by the diffusion factor D do not explain the higher losses measured in the rotor of reference 1.

Inlet relative Mach number levels are about equal for both compressor rotors; therefore, this parameter itself does not explain the difference in the loss levels. The axial velocity ratios measured in the tests of the rotors of reference 1 were about 0.8 at a tip speed of 1000 feet per second; whereas, the measured axial velocity ratios of the present rotors are 0.9 or greater. It is possible that a lower axial velocity ratio supplements the effect of solidity on losses and causes the high losses in the rotors of reference 1 at the lower solidity levels. However, such a conjecture should not be accepted without further verification, because axial velocity ratio may represent only one of the differences between the two investigations that may affect losses.

Therefore, there are two major observations, the increase in tip-section losses with a decrease in solidity and the comparison of tip-section losses in two separate solidity investigations, which cannot be explained on the basis of conventional flow parameters of inlet relative Mach number, diffusion factor, and axial velocity ratio. Evidently, a change in solidity alters the flow field about the tip section in such

4002

a manner that changes in the conventional flow parameters computed from inlet and outlet conditions do not explain the loss phenomena.

Suction-surface Mach number level. - For operation of a low-solidity cascade at high relative inlet Mach numbers, the suction-surface velocity profile could be of a form such that the diffusion factor does not provide a correct estimate of the blade loading and the resulting blade profile losses. That is, the velocity profile could be considerably different from the model on which the diffusion-factor analysis was based (ref. 7). Furthermore, the diffusion and losses caused by shock waves may also become important at low solidity levels.

In this section the effects of solidity on tip-section losses are estimated by computing suction-surface velocities. Figure 11 shows for discussion purposes a simplified picture of two-dimensional flow about a cascade of airfoils for two solidity levels (1.00 and 0.63) corresponding to the tip sections of the 35- and 22-blade rotors. For both solidity levels, a design-speed (supersonic inlet relative velocity) operating condition with back pressure was chosen; hence, a detached bow wave of the form shown is assumed.

Blade surface Mach numbers were computed by means of a two-dimensional Prandtl-Meyer expansion (assuming no losses), and figure 11 shows Mach numbers for the suction surfaces just upstream of the shock wave. These Mach numbers indicate the relative strength of the shock waves at the suction surface for the two solidity levels. The lower solidity has the greater blade surface Mach number; hence, greater losses should be anticipated for the low solidity, since the total-pressure loss across a shock increases with increasing Mach number. The chance for a flow separation (another source of high losses) is also greater in the low-solidity cascade, because the static-pressure rise across the shock wave increases with increasing Mach number and the shock wave hits closer to the trailing edge where the boundary layer may be in a poor condition to withstand a sudden increase in static pressure.

Surface Mach number values offer one explanation for the increase in tip-section losses with decreasing solidity at high speeds for this investigation. Figure 8 also shows that, at low speeds, the losses do not vary with solidity. At the low inlet relative Mach numbers, surface Mach numbers are low and shock waves do not exist or are very weak. Thus, the suction-surface Mach number analysis of loss trends does not contradict the low-speed test results.

Computed tip-section surface Mach numbers were 1.74 for the low-solidity rotor of reference 1 operating at a corrected tip speed of 1000 feet per second (inlet relative Mach number equal to 1.06). This compares with a value of 1.61 computed for the low-solidity rotor of the present investigation. The higher surface Mach number level and the

subsequent stronger normal shock may account for the higher losses
measured in the low-solidity rotor of reference 1 as shown in figure 10.
The higher values of suction-surface Mach number reported in reference 1
arise from the comparatively high tip-section camber angles of those
rotors.

Deviation Angles

    In the design of high-speed compressors, close control over the
rotor-outlet flow direction is required if design total-pressure ratio
is to be obtained (ref. 9). Deviation angle δ^O (fig. 1) has been used
to define the outlet flow direction from blade rows constructed with
double-circular-arc airfoils. Previous rotor test results (refs. 1, 4,
and 6) show that Carter's rule (ref. 9) can be used to predict design-
point deviation angles for circular-arc compressor blades. Carter's
rule was derived from low-speed two-dimensional-cascade data and is
written as

$$\delta^O = m_c \; \varphi \; \sqrt{\frac{1}{\sigma}} \tag{2}$$

where m_c depends on chord angle and is constant for one blade element,
and the camber angle φ is also fixed for a given blade element.
Equation (2) predicts an increase in tip-section deviation angle of 0.5^O
as the solidity σ is decreased from 1.00 to 0.63. Hub-section deviation
angles (according to Carter's rule) should increase 1.5^O as solidity is
decreased from 1.61 to 1.01. These changes in deviation angle with
solidity are of the same order as the probable error of a single measure-
ment of deviation angle.

    Variation of deviation angle with incidence angle. - Figure 12
presents a comparison of deviation-angle variation with incidence angle
for the three solidities for hub, mean, and tip blade-element sections.
At the hub section (fig. 12(a)), deviation angle increases with increas-
ing incidence angle for all speeds. This does not agree with low-speed
two-dimensional-cascade results. For solidities over 1.0 (hub section),
available cascade tests indicate that deviation angles should not vary
with incidence angle, at least in the operating range of low-loss
incidence angle. There is no evident explanation for this discrepancy
between rotor and cascade results.

    At the mean section (fig. 12(b)), the deviation-angle trend to
decrease with decreasing incidence angle appears only at 60 and 80 percent
of design speed for the two lower solidities. For the other data, the
deviation-angle variation is similar to the loss-coefficient variation
with incidence angle.

    At the tip section (fig. 12(c)), the similarity between deviation-
angle and loss variation with incidence angles is present at all speeds

for the three solidities. The general level of deviation angles at the
tip section is also substantially lower for the other blade-element
sections because of the low tip-section camber angle.

Deviation angles at minimum-loss incidence angles. - Measured
deviation angles at minimum-loss incidence angles (taken from faired
curves in figs. 6 and 7) are compared with Carter's rule values in
figure 13. The measured deviation angles are plotted against percent
of design speed merely to catalog the data. Carter's rule was derived
for optimum-incidence-angle operation (defined as the incidence angle
at which the cascade turning angle is 0.8 of the maximum turning angle).
Whether rotor minimum-loss incidence angles coincide with cascade
optimum incidence angles is questionable. However, the differences are
probably small, and in many cases deviation angle does not vary much
with incidence angle in the minimum-loss range. An exception is the hub
section of this rotor (fig. 12(a)).

For the hub section (fig. 13(a)), the deviation-angle data scattered,
but the general level agrees fairly well with Carter's rule values.
Because of the data scatter, no sign of a definite solidity effect can
be seen. It should be noted that accurate control of the relative outlet
flow direction (deviation angle) is not required for hub sections
because of the low wheel speed and the nearly axial relative discharge
velocity (ref. 9).

At the mean section (fig. 13(b)), the measurements show no definite
solidity effect, and deviation angles vary just slightly with speed. The
general level of the measured deviation angles for all solidities is
about the same level as the Carter's rule values.

At the tip section (fig. 13(c)), the deviation angles for the
highest solidity check Carter's rule well, and only a small variation
with speed is evident. The deviation angles for the two lower solidities
at 80 percent of design speed and below are less than the deviation-
angle values of the high-solidity rotor. Such a variation, which is
counter to Carter's rule, may be due to measurement errors. Above 80 per-
cent of design speed, the deviation angles of the two lower-solidity
rotors increase with speed and become greater than the deviation angles
for the high-solidity rotor. The increase in deviation angle with speed
may be due to flow separation, which could also cause the high losses
discussed previously.

SUMMARY OF RESULTS

In order to obtain more data on the effects of solidity on perform-
ance of transonic compressor rotors operating at inlet relative Mach
numbers in the neighborhood of 1.1, two lower-solidity configurations

NACA RM E56D06

of the 1.5-inch-chord transonic compressor rotor were tested. Except for
the number of blades, the two lower-solidity rotors were identical with
the original rotor. The original rotor had 35 blades with solidity at
the outer wall of 0.95; the two low-solidity rotors had 28 and 22 blades,
with solidities of 0.76 and 0.60, respectively. The blade-element per-
formance of the two low-solidity rotors was generally similar to that of
the original 35-blade rotor and previously published transonic-compressor
rotor data. The following results were obtained in this investigation:

1. Comparison of hub and mean blade-element loss coefficients for
three solidity levels showed no consistent variation with solidity.
Loss levels for the three solidities were low.

2. Rotor tip-section (10 percent of the passage height away from the
outer wall) minimum-loss levels did not vary with solidity at low relative
inlet Mach numbers (60 and 80 percent of design rotor speed). At high
relative inlet Mach numbers (90 and 100 percent of design rotor speed)
tip-section losses increased with decreasing solidity contrary to the
trends shown by low-speed two-dimensional-cascade data.

3. Diffusion factor and inlet relative Mach number level did not
explain the variation in tip-section losses with solidity. However, the
suction-surface Mach number, computed by the Prandtl-Meyer method, offered
a reason for the observed increase in loss with a decrease in solidity.

4. The measured deviation angles for the 35-, 28-, and 22-blade rotors
agreed fairly well with Carter's rule values for operation at the minimum-
loss incidence angle of the rotors. Deviation angles at minimum-loss
incidence angle did not vary significantly with speed except for the tip
section of the two low-solidity rotors. In this instance, deviation
angles tend to increase with speed.

5. Periodic rotating stall did not occur in the low-solidity rotors
at speeds of 50, 60, and 80 percent of design. Instead, only random flow
fluctuations appeared as the flow was reduced into the stalled operating
range. Periodic rotating stalls were observed in previous tests of the
high-solidity rotor.

Lewis Flight Propulsion Laboratory
    National Advisory Committee for Aeronautics
        Cleveland, Ohio, April 10, 1956

<div align="center">REFERENCES</div>

1. Schwenk, Francis C., and Lewis, George W., Jr.: Experimental Inves-
    tigation of a Transonic Axial-Flow-Compressor Rotor with Double-
    Circular-Arc Airfoil Blade Sections. III - Comparison of Blade-
    Element Performance with Three Levels of Solidity. NACA RM E55F01,
    1955.

2. Tysl, Edward R., Schwenk, Francis C., and Watkins, Thomas B.: Experimental Investigation of a Transonic Compressor Rotor with a 1.5-Inch Chord Length and an Aspect Ratio of 3.0. I - Design, Over-All Performance, and Rotating-Stall Characteristics. NACA RM E54L31, 1955.

3. Schwenk, Francis C., and Tysl, Edward R.: Experimental Investigation of a Transonic Compressor Rotor with a 1.5-Inch Chord Length and an Aspect Ratio of 3.0. II - Blade-Element Performance. NACA RM E55F10, 1955.

4. Schwenk, Francis C., Lieblein, Seymour, and Lewis, George W., Jr.: Experimental Investigation of an Axial-Flow Compressor Inlet Stage Operating at Transonic Relative Inlet Mach Numbers. III - Blade-Row Performance of Stage with Transonic Rotor and Subsonic Stator at Corrected Tip Speeds of 800 and 1000 Feet Per Second. NACA RM E53G17, 1953.

5. Lieblein, Seymour: Review of High-Performance Axial-Flow-Compressor Blade-Element Theory. NACA RM E53L22, 1954.

6. Robbins, William H., and Glaser, Frederick W.: Investigation of an Axial-Flow-Compressor Rotor with Circular-Arc Blades Operating Up to a Rotor-Inlet Relative Mach Number of 1.22. NACA RM E53D24, 1953.

7. Lieblein, Seymour, Schwenk, Francis C., and Broderick, Robert L.: Diffusion Factor for Estimating Losses and Limiting Blade Loadings in Axial-Flow-Compressor Blade Elements. NACA RM E53D01, 1953.

8. Herrig, L. Joseph, Emery, James C., and Erwin, John R.: Systematic Two-Dimensional Cascade Tests of NACA 65-Series Compressor Blades at Low Speeds. NACA RM L51G31, 1951.

9. Carter D. S.: The Low Speed Performance of Related Aerofoils in Cascade. Rep. No. R.55, British N.G.T.E., Sept. 1949.

4002

TABLE I. - MEASURED ROTOR BLADE-ELEMENT GEOMETRY

Radius, in.		Solidity, σ			Measured blade angle, deg	
Inlet, r_3	Outlet, r_4	35-Blade rotor	28-Blade rotor	22-Blade rotor	Inlet, κ_3	Outlet, κ_4
9.00	9.00	0.95	0.76	0.60	----	----
8.54	8.60	1.00	.80	.63	50.6	44.6
8.27	8.36	1.03	.82	.65	49.8	42.8
7.90	8.04	1.07	.86	.67	48.6	40.0
7.49	7.68	1.13	.90	.71	47.1	36.5
6.71	7.00	1.25	1.00	.79	44.2	28.9
5.93	6.32	1.40	1.12	.88	41.0	20.0
5.15	5.64	1.61	1.29	1.01	37.7	9.4
4.50	5.00	1.89	1.51	1.19	----	----
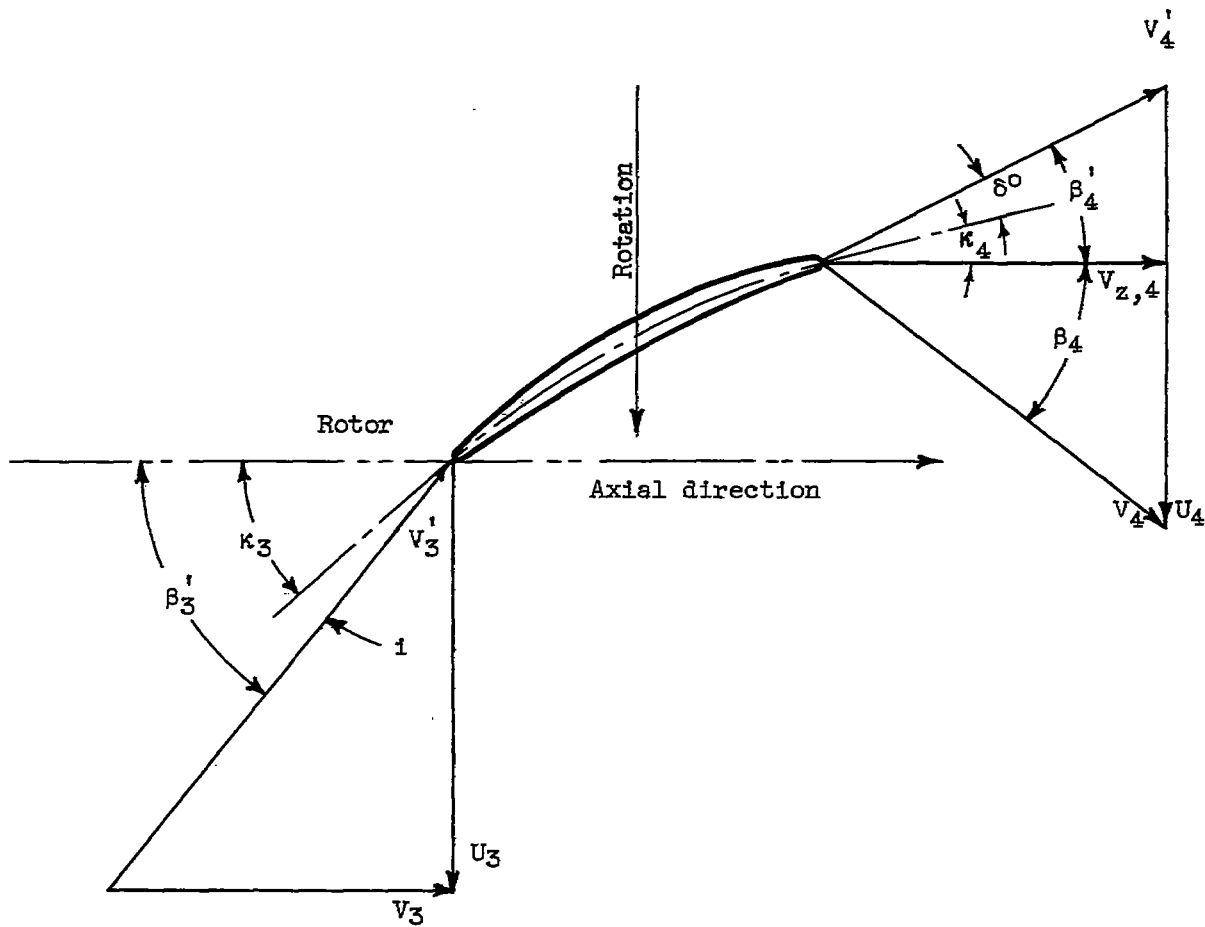
Figure 1. - Velocity-diagram notation for blade element.

Collector

Rotor

Air
flow →

Static-
pressure
rake

2 3   4

CD-3611

Station 1
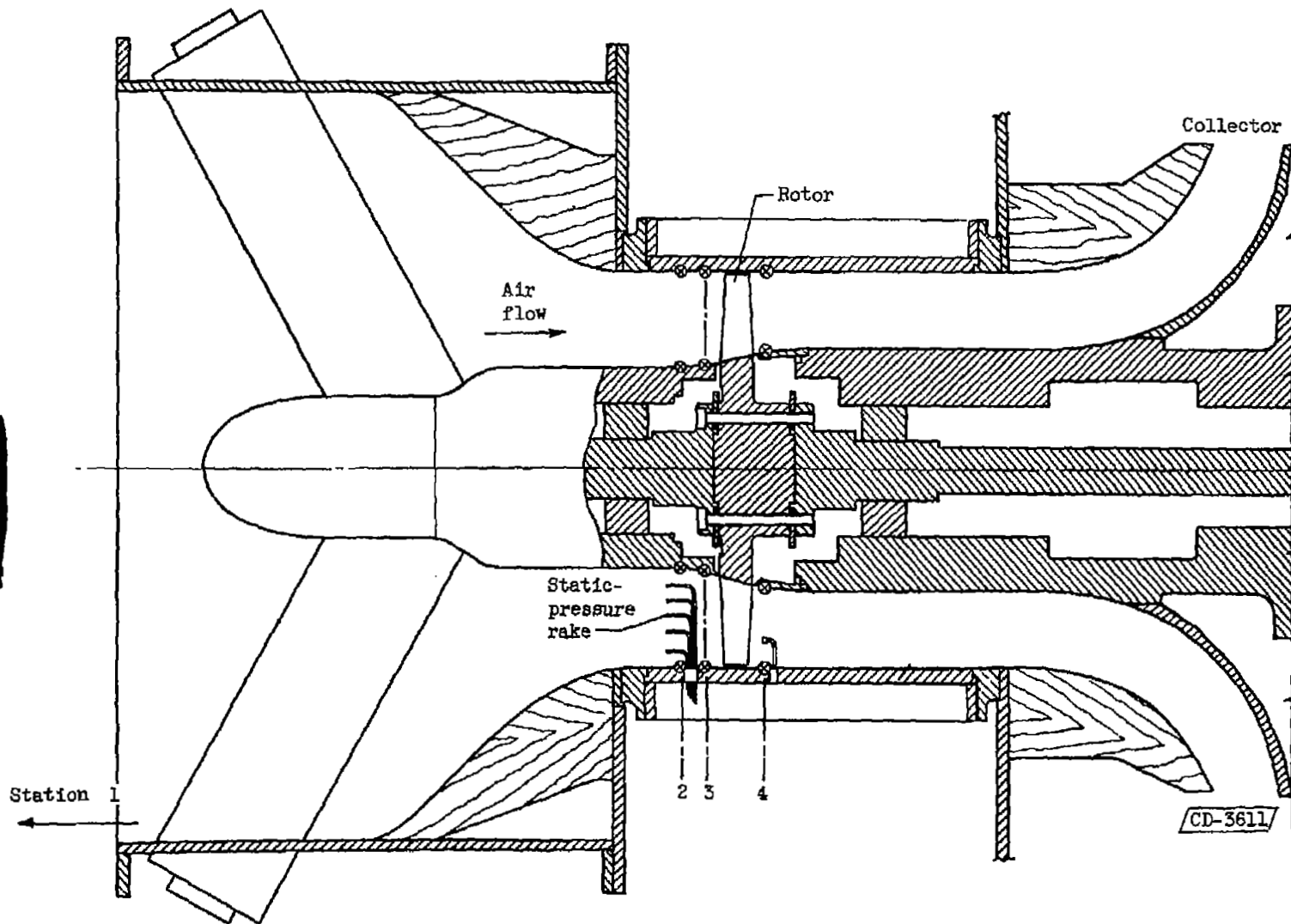
Figure 2. - Schematic diagram of variable-component transonic-compressor test rig.

4002

CW-3 back

(a) Corrected tip speed, 100-percent design.

(b) Corrected tip speed, 90-percent design.

Blades	Rotor tip solidity, σ_t
○ 35	0.95
□ 28	.76
◇ 22	.60

Corrected specific weight flow, $w\sqrt{\theta}/\delta A_F$, (lb/sec)/sq ft

(c) Corrected tip speed, 80-percent design.
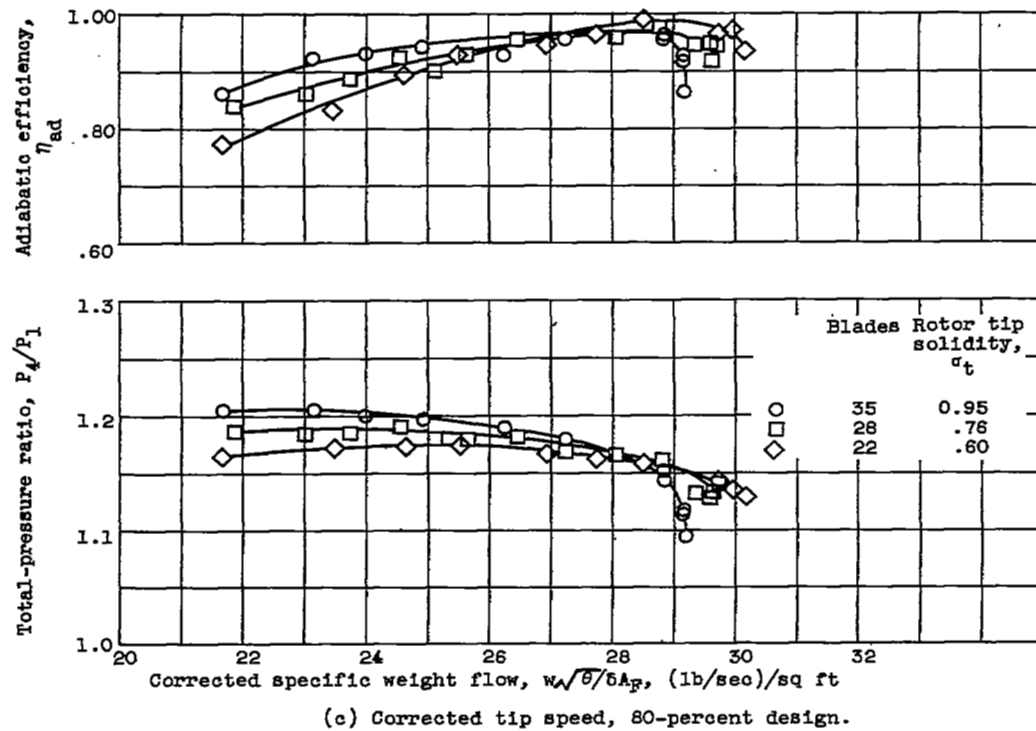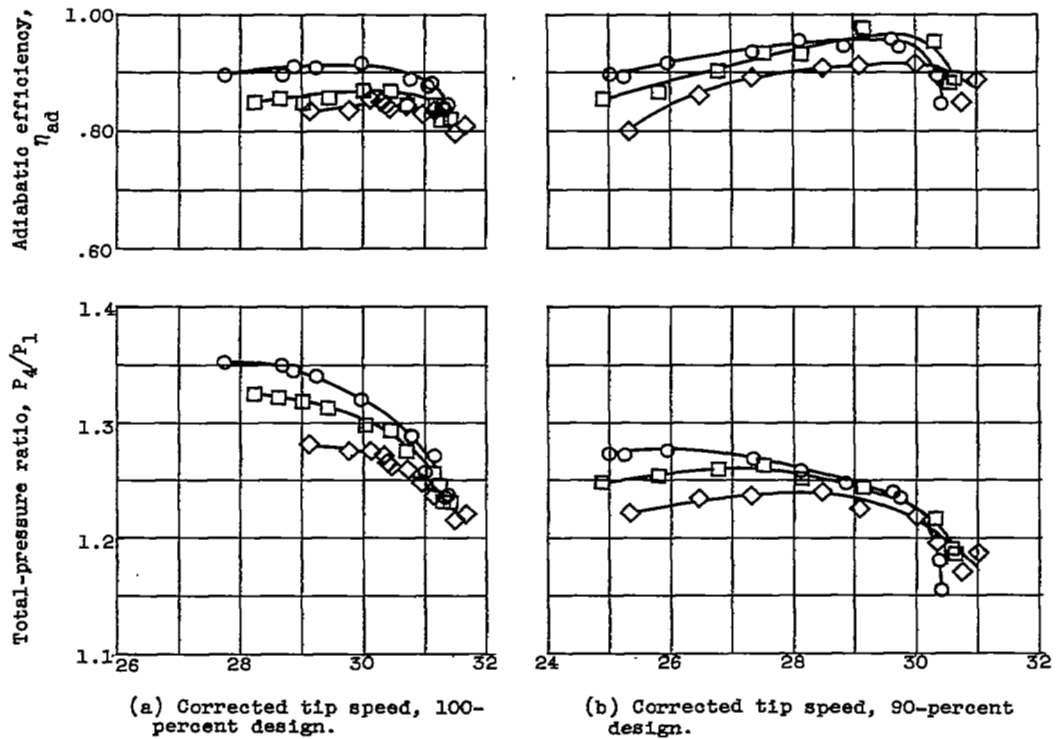
Figure 3. – Comparison of mass-averaged rotor performance at three solidity levels for 1.5-inch-chord transonic compressor rotor.
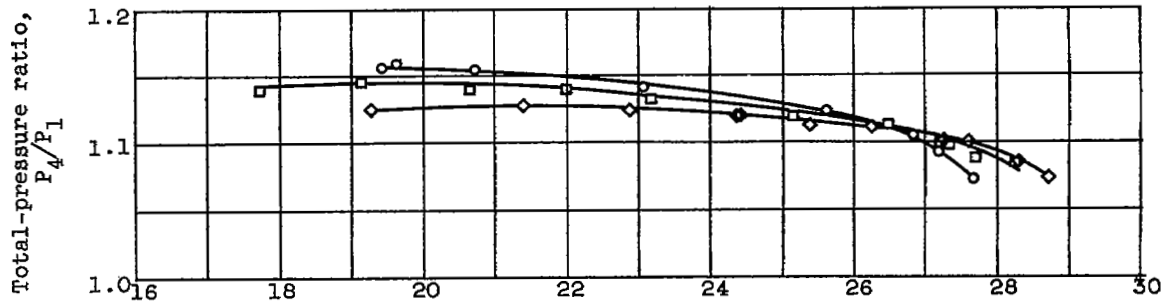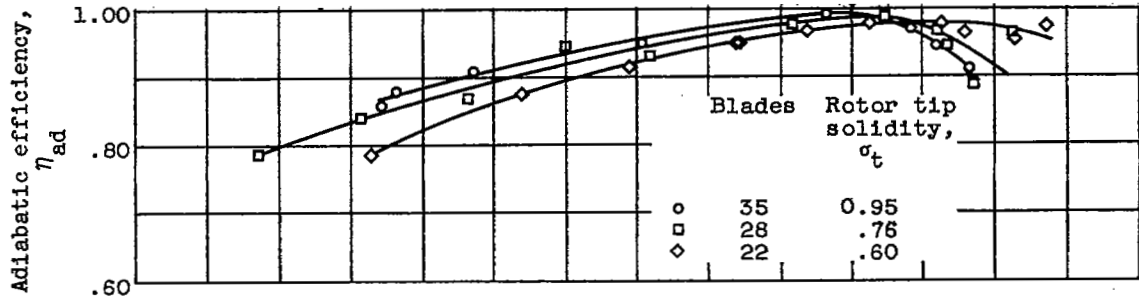
(d) Corrected tip speed, 70-percent design.
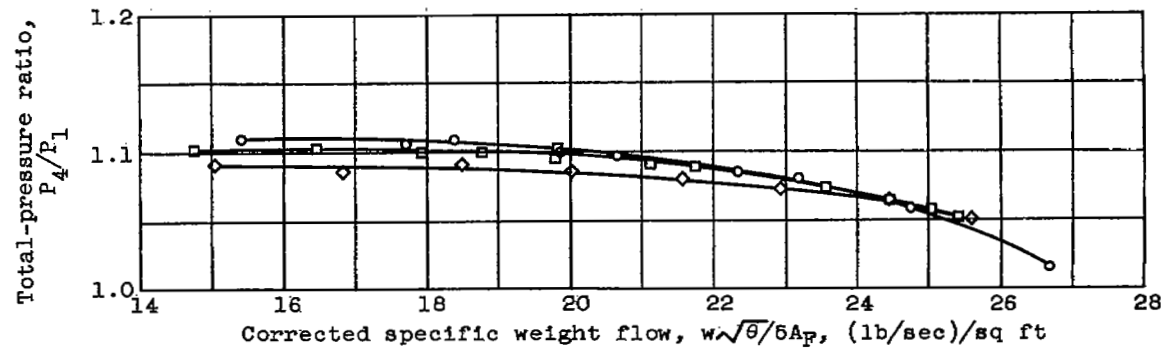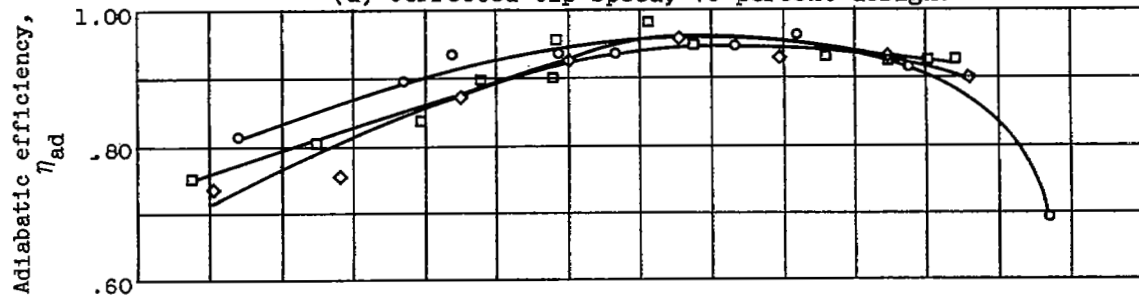
(e) Corrected tip speed, 60-percent design.

Figure 3. - Concluded. Comparison of mass-averaged rotor performance at three solidity levels for 1.5-inch-chord transonic compressor rotor.
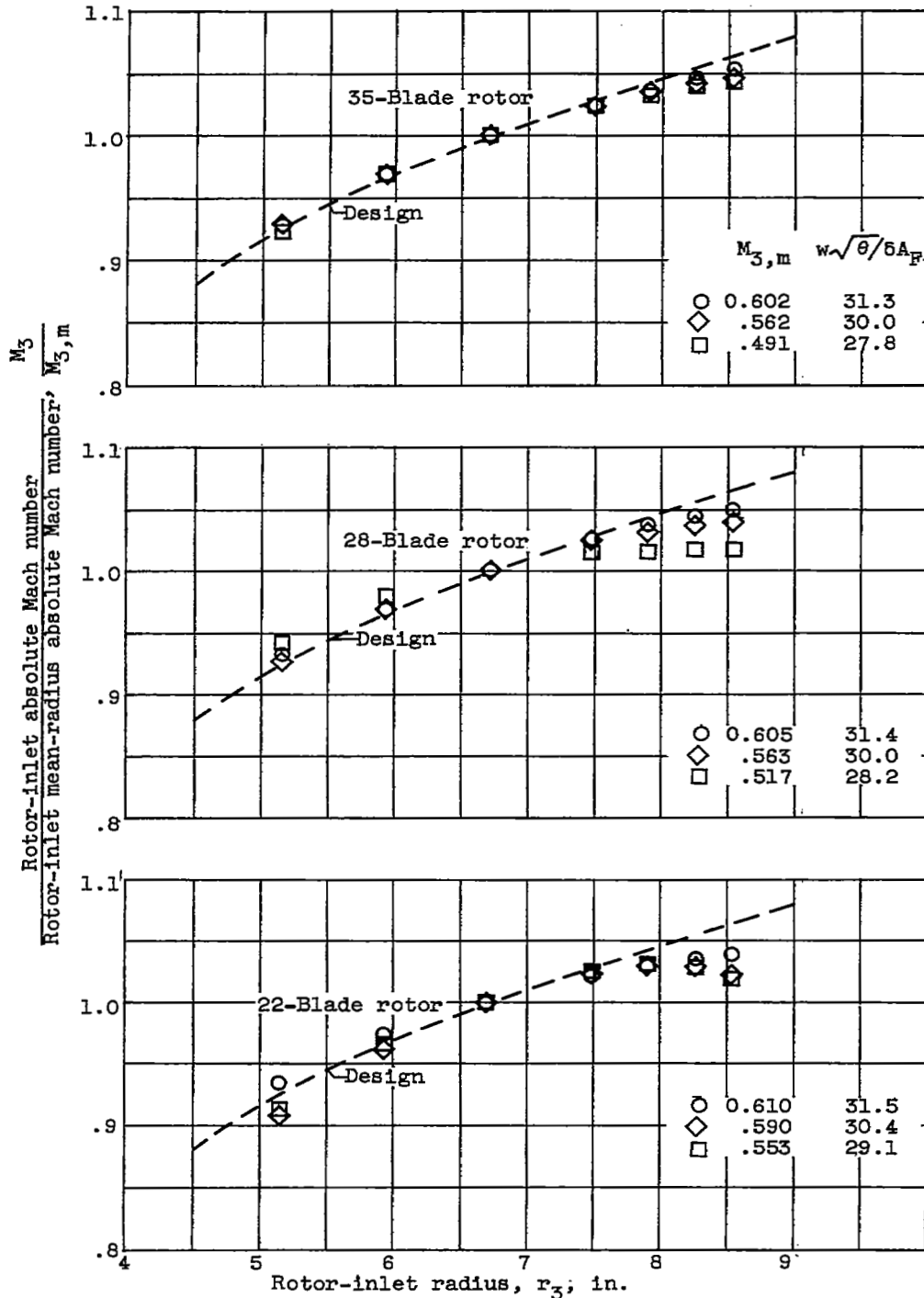
(a) Corrected tip speed, 100-percent design.

Figure 4. - Radial variation of rotor-inlet absolute Mach number.
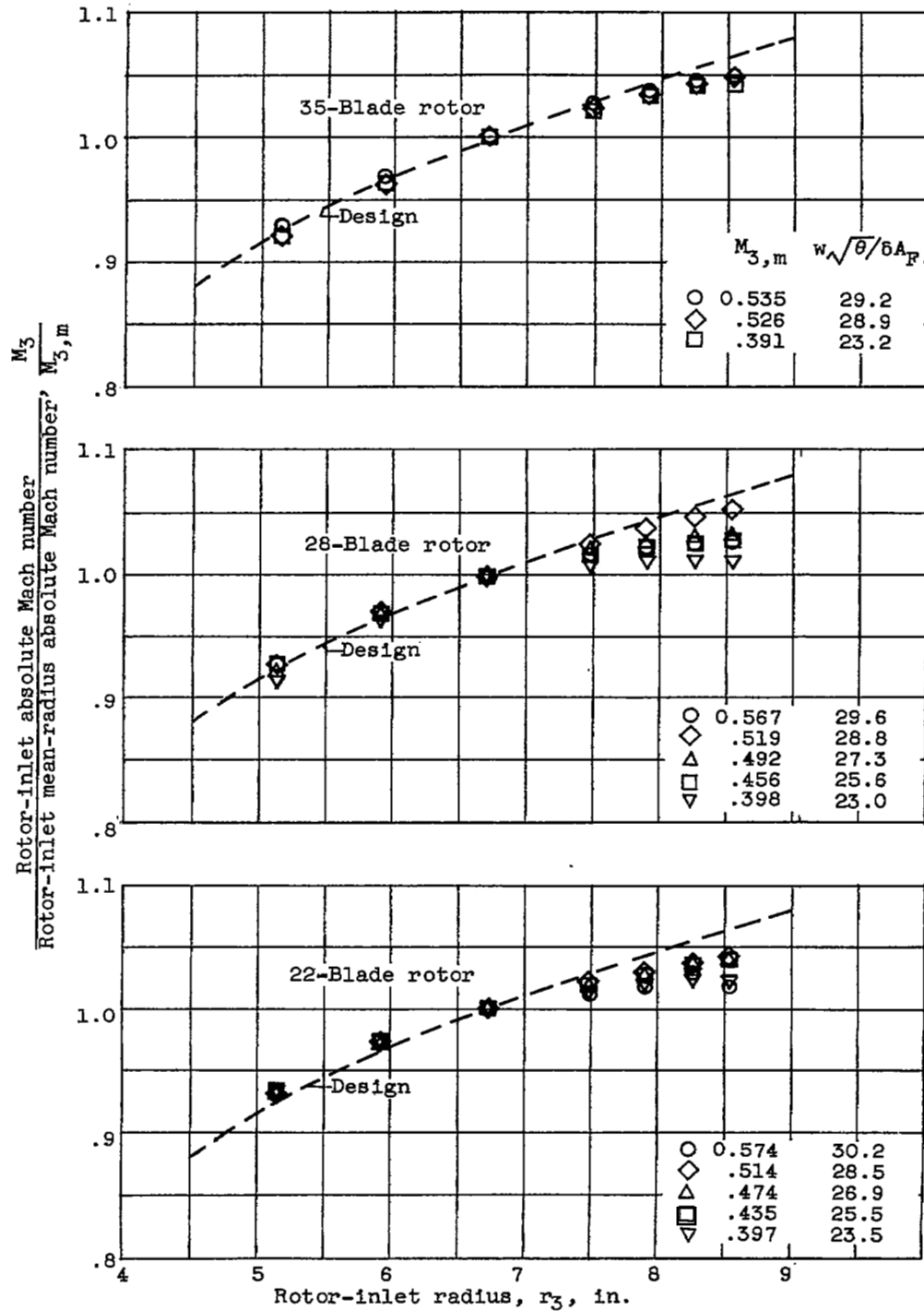
(b) Corrected tip speed, 80-percent design.

Figure 4. - Concluded. Radial variation of rotor-inlet absolute Mach number.

4002
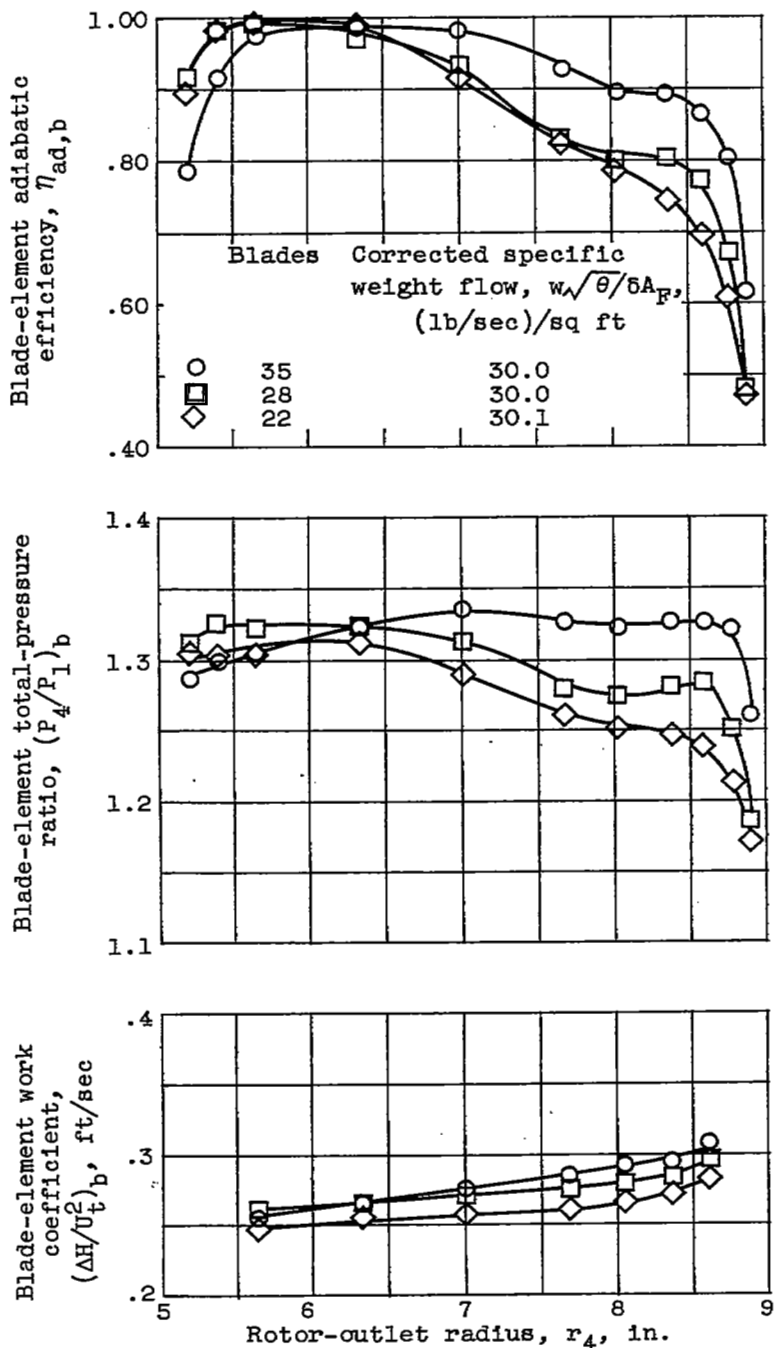
(a) Corrected tip speed, 100-percent de-
sign. Near peak-efficiency operating
condition.

Figure 5. - Radial variation of blade-
element data for three solidity
levels.
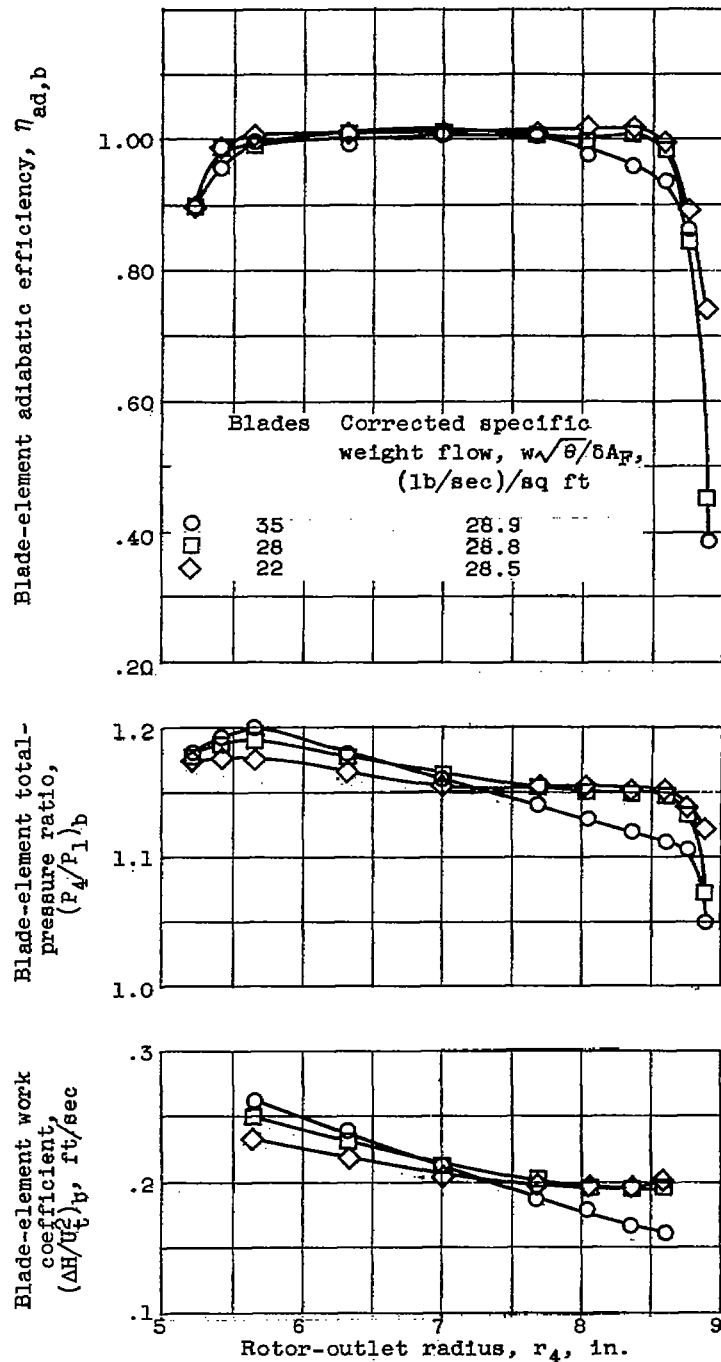
(b) Corrected tip speed, 80-percent design. High weight flow. Near peak-efficiency operating condition.

Figure 5. - Continued. Radial variation of blade-element data for three solidity levels.
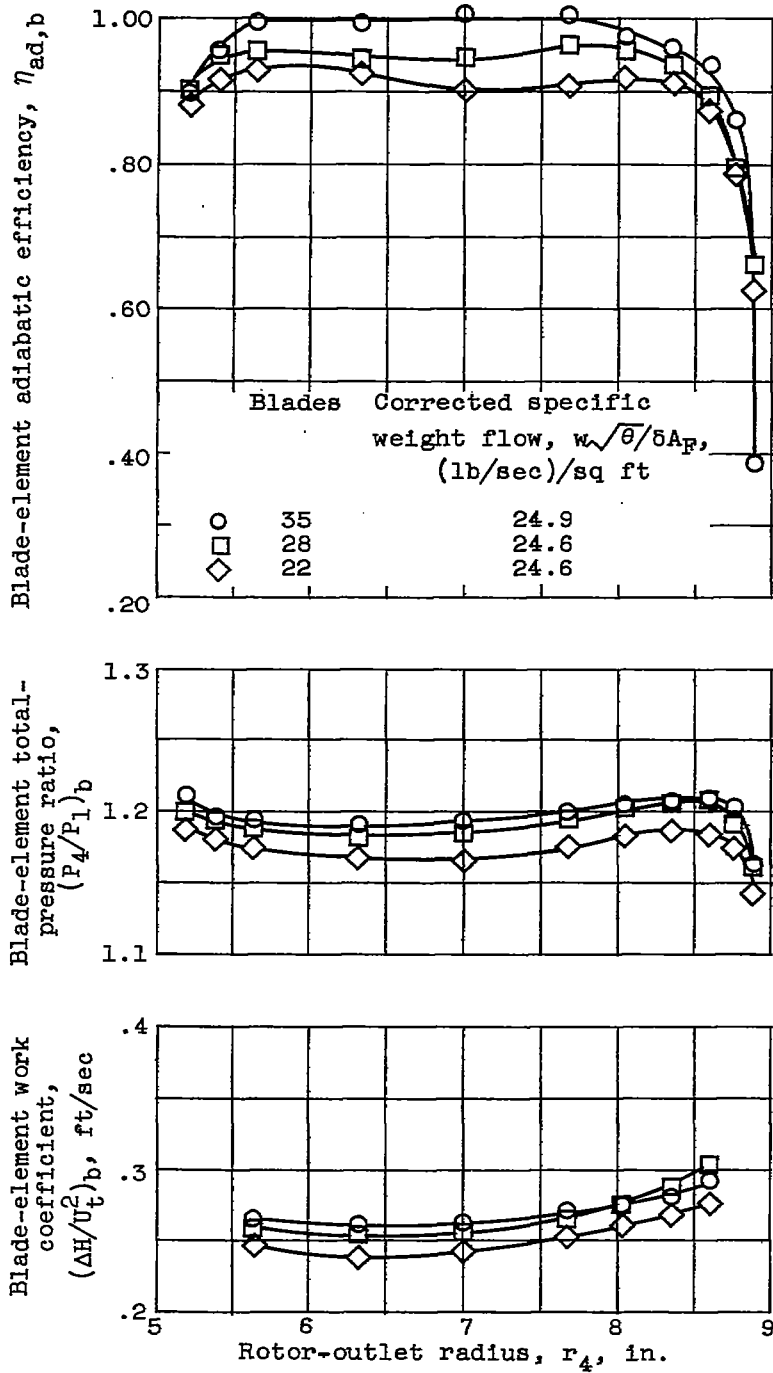
(c) Corrected tip speed, 80-percent de-
sign. Reduced weight flow.

Figure 5. - Concluded. Radial variation
of blade-element data for three solid-
ity levels.

(a) Hub section (r_4 = 5.64 in.).
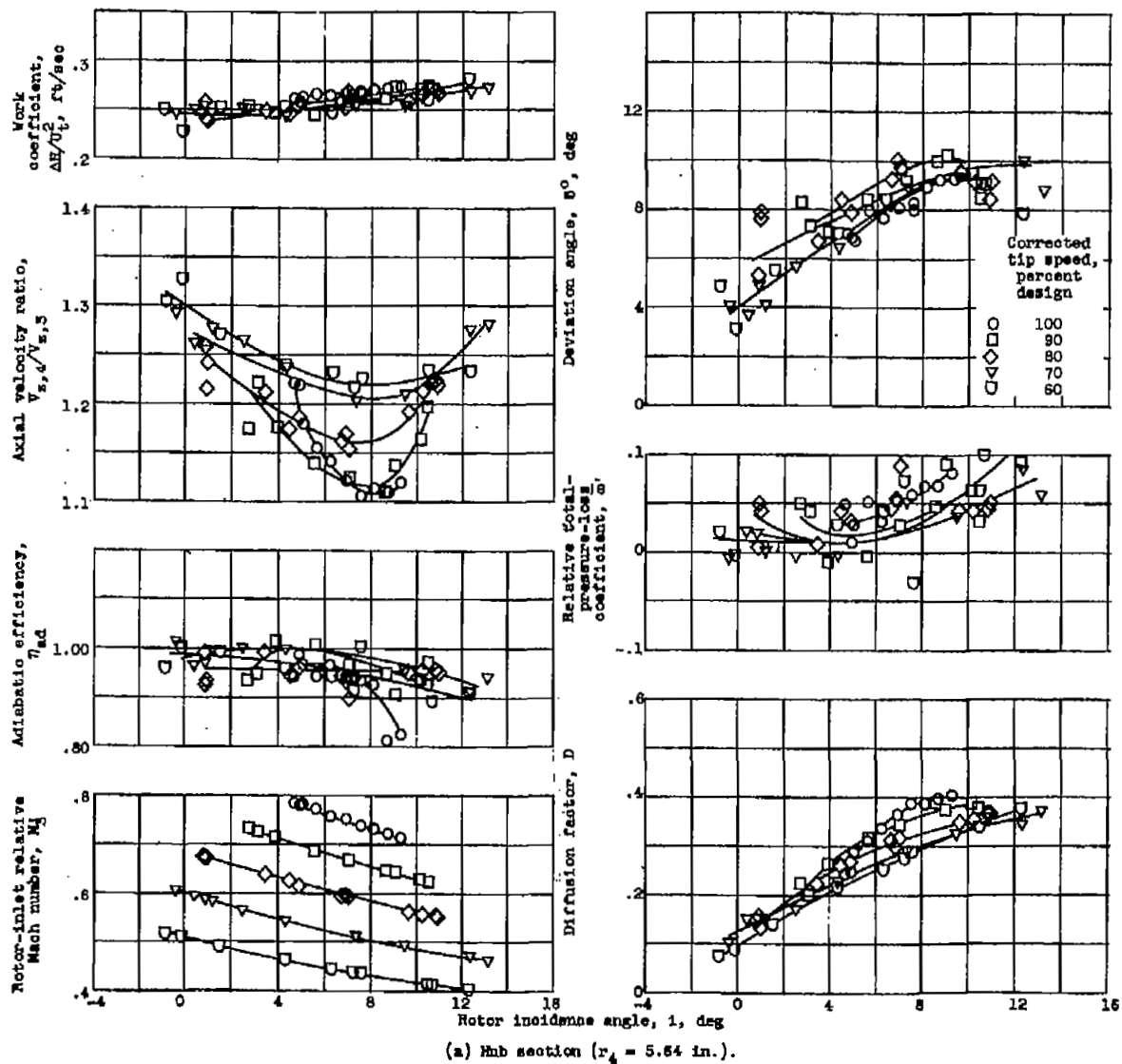
Figure 6. - Rotor blade-element characteristics for 28-blade 1.5-inch-chord transonic compressor rotor at various speeds.

4002

CW-4 back

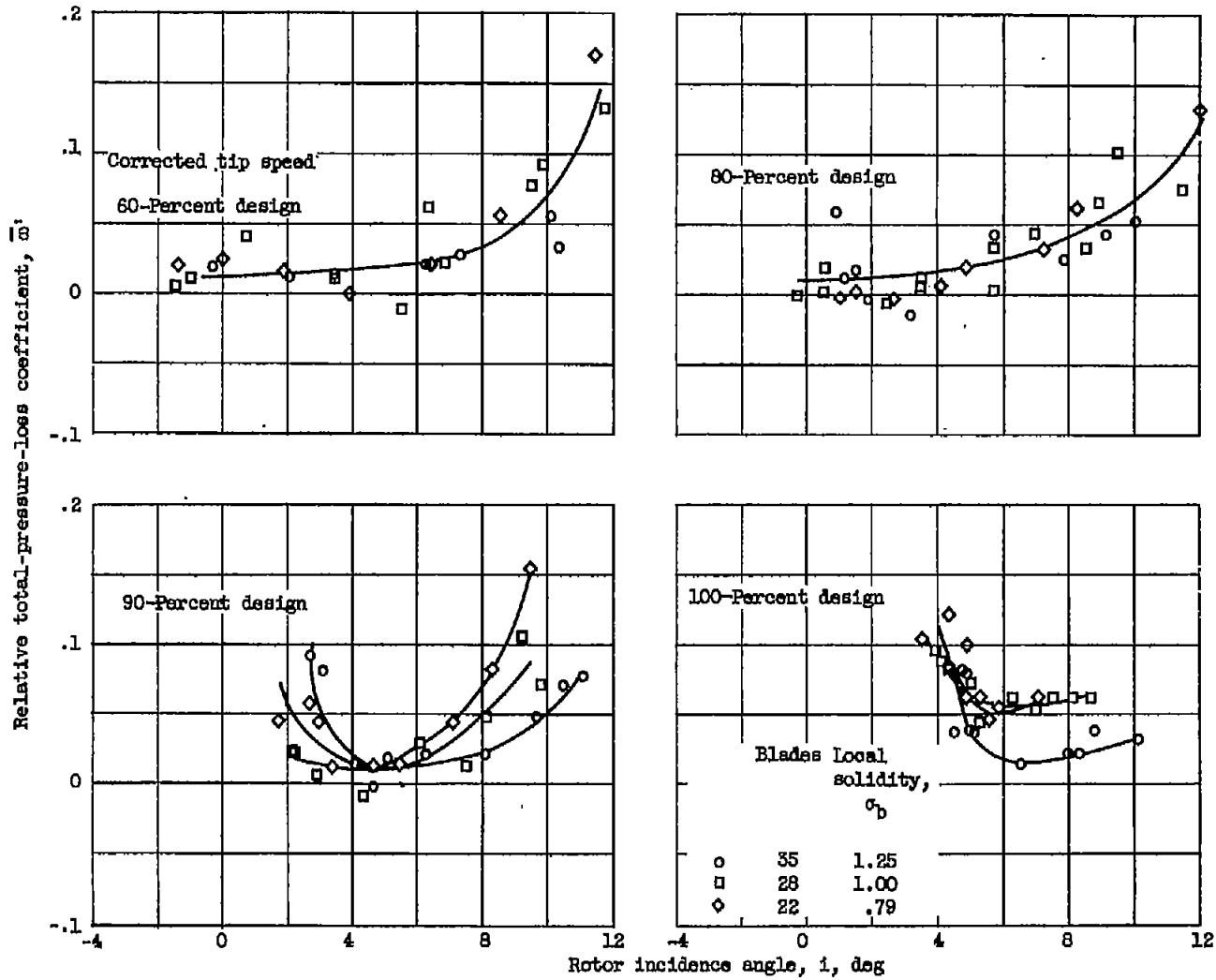

(b) Mean section (r_4 = 7.00 in.).

Figure 6. - Continued. Rotor blade-element characteristics for 28-blade 1.5-inch-chord transonic compressor rotor at various speeds.

(c) Tip section ($r_4 = 8.60$ in.)

Figure 6. – Concluded. Rotor blade-element characteristics for 28-blade 1.5-inch-chord transonic compressor rotor at various speeds.

4002

Rotor incidence angle, i, deg
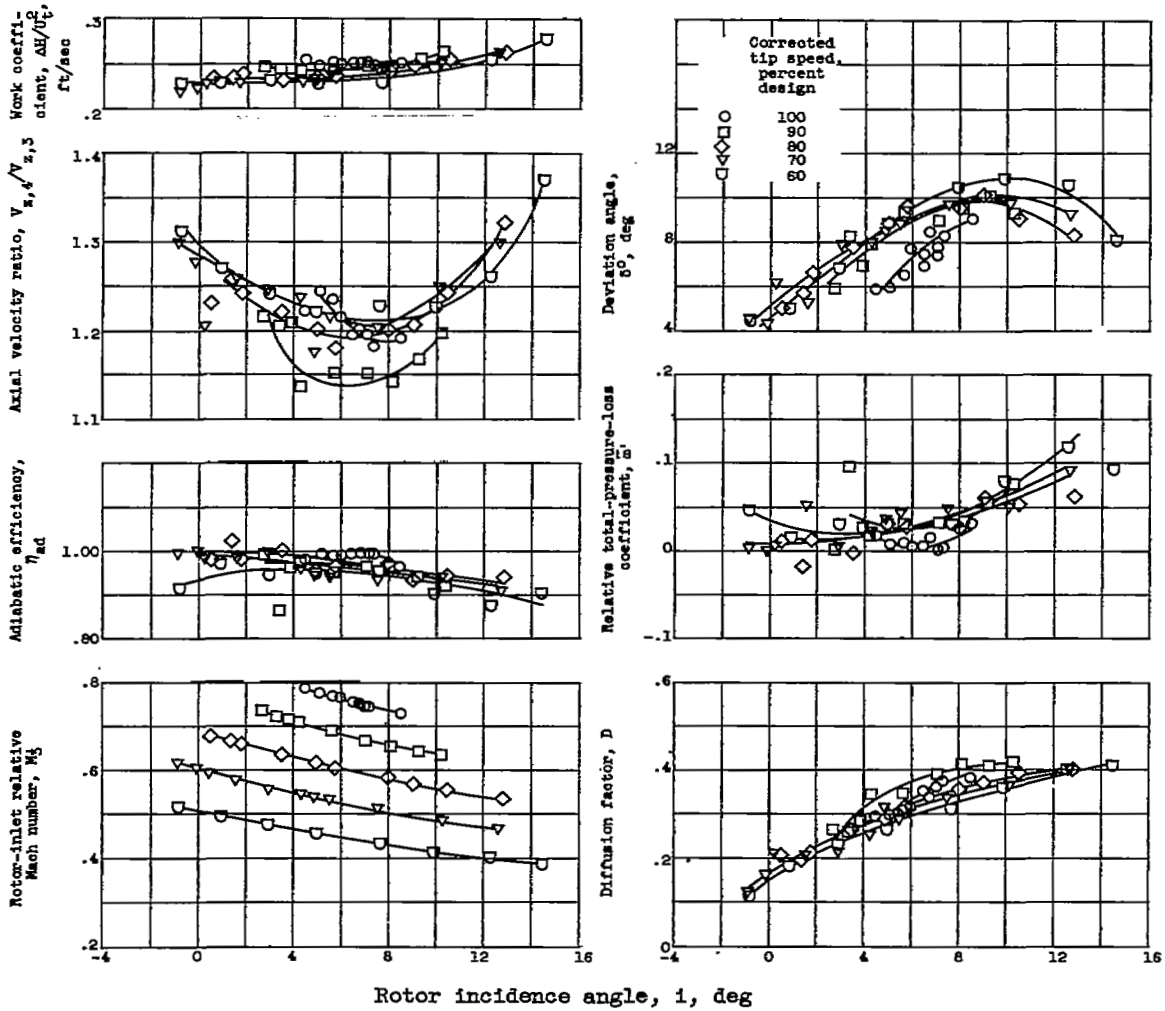
(a) Hub section (r_4 = 5.64 in.).

Figure 7. - Rotor blade-element characteristics for 22-blade 1.5-inch-chord transonic compressor rotor at various speeds.
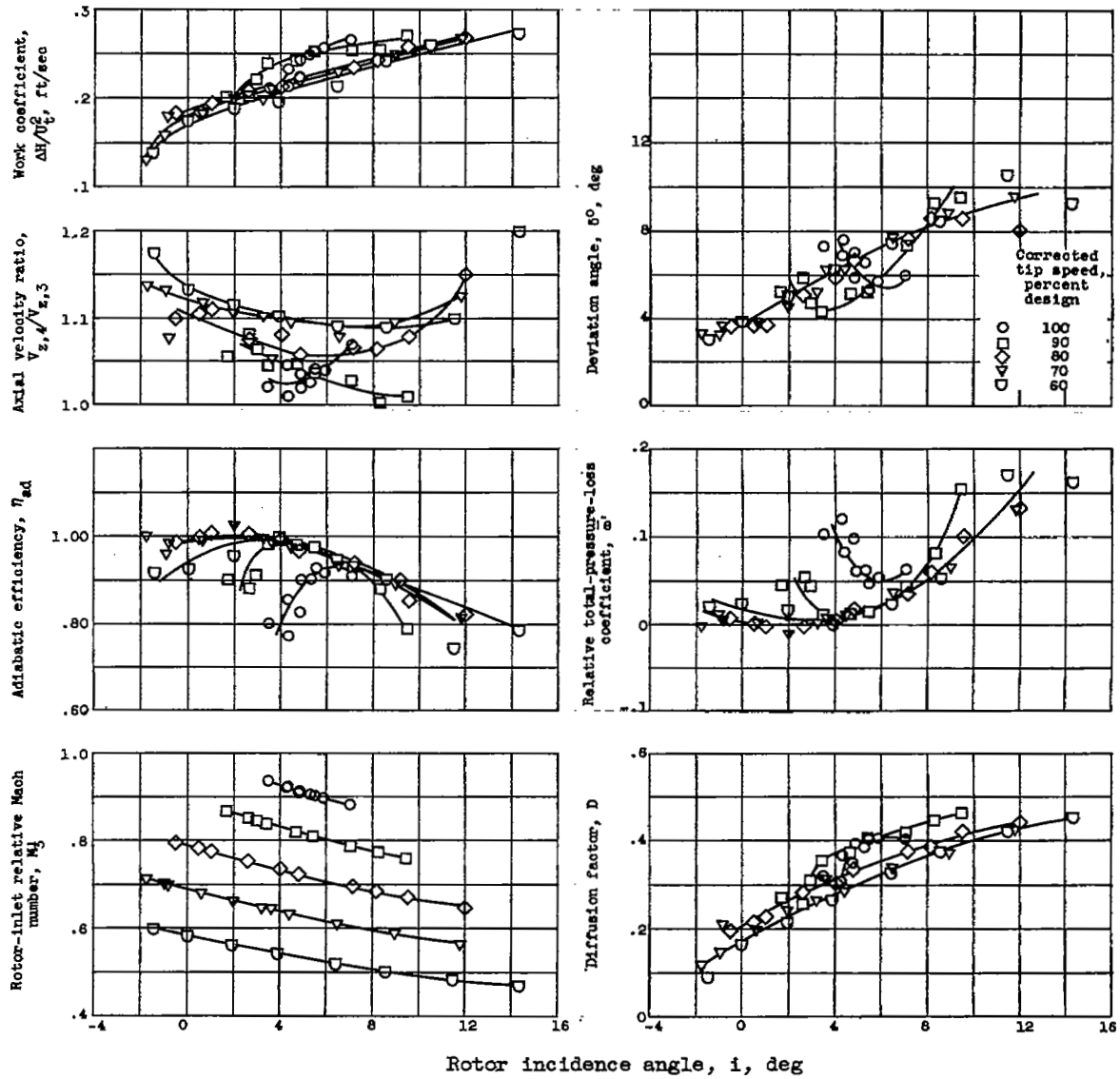
(b) Mean section ($r_4 = 7.00$ in.).

Figure 7. - Continued. Rotor blade-element characteristics for 22-blade 1.5-inch-chord transonic compressor rotor at various speeds.

4002

Rotor incidence angle, i, deg
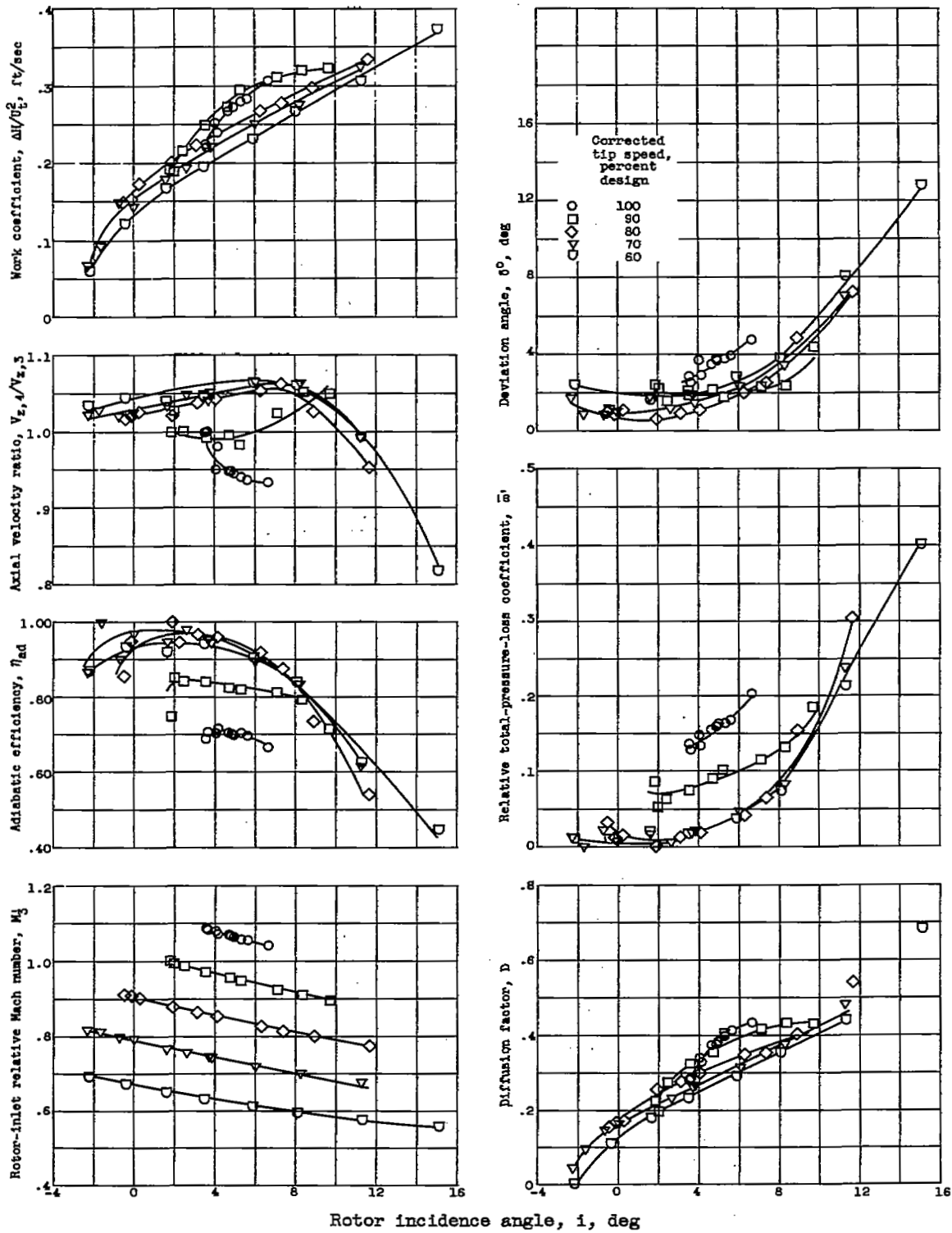
(c) Tip section (r_4 = 8.60 in.).

Figure 7. - Concluded. Rotor blade-element characteristics for 22-blade 1.5-inch-chord transonic compressor rotor at various speeds.
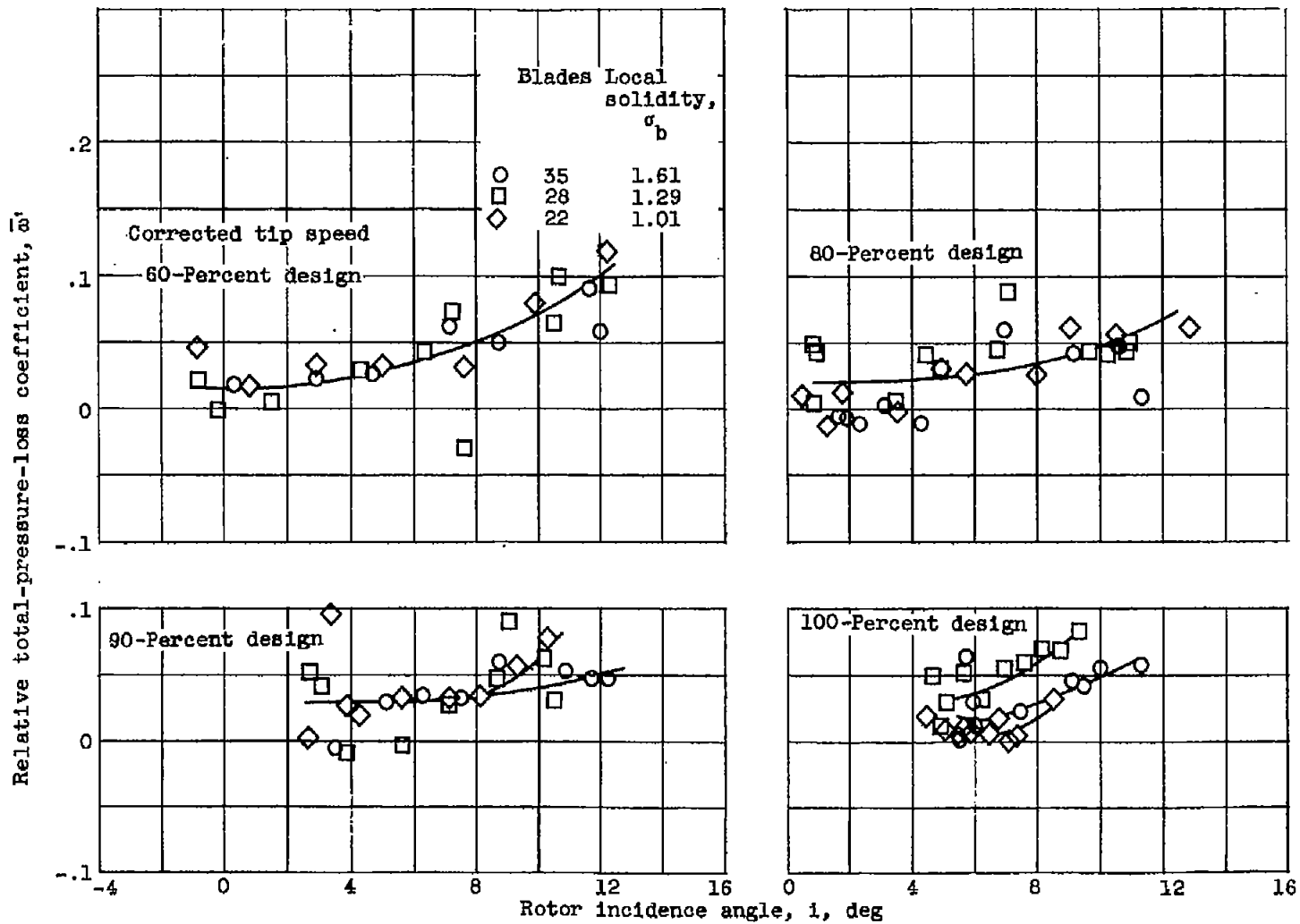
(a) Hub section (r_4 = 5.64 in.).

Figure 8. - Comparison of loss-coefficient variation with incidence angle for three solidity levels of 1.5-inch-chord transonic compressor rotor.

(b) Mean section (r_4 = 7.00 in.).

Figure 8. - Continued. Comparison of loss-coefficient variation with incidence angle for three solidity levels of 1.5-inch-chord transonic compressor rotor.
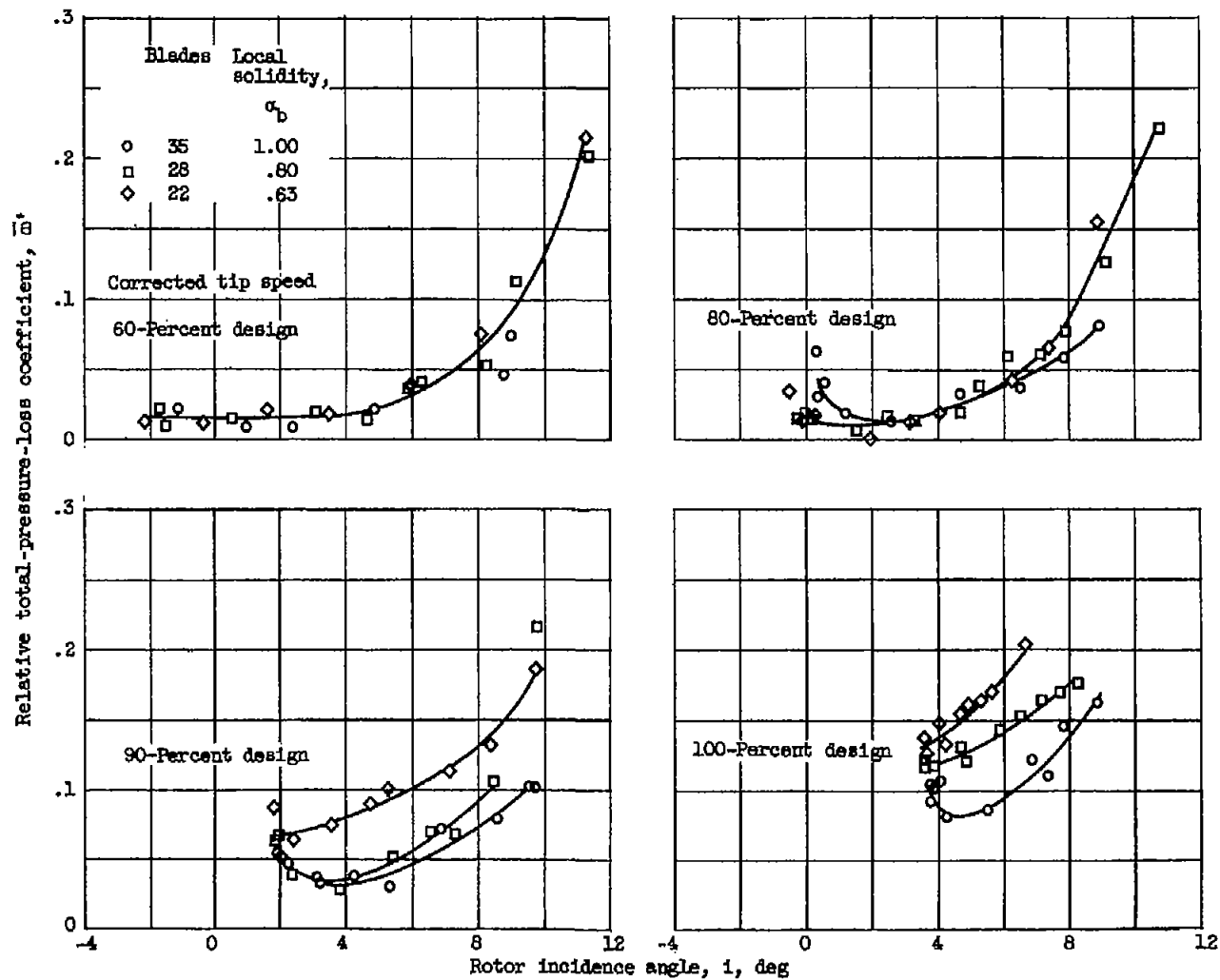
(c) Tip section (r_4 = 8.60 in.).

Figure 8. - Concluded. Comparison of loss-coefficient variation with incidence angle for three solidity levels of 1.5-inch-chord transonic compressor rotor.
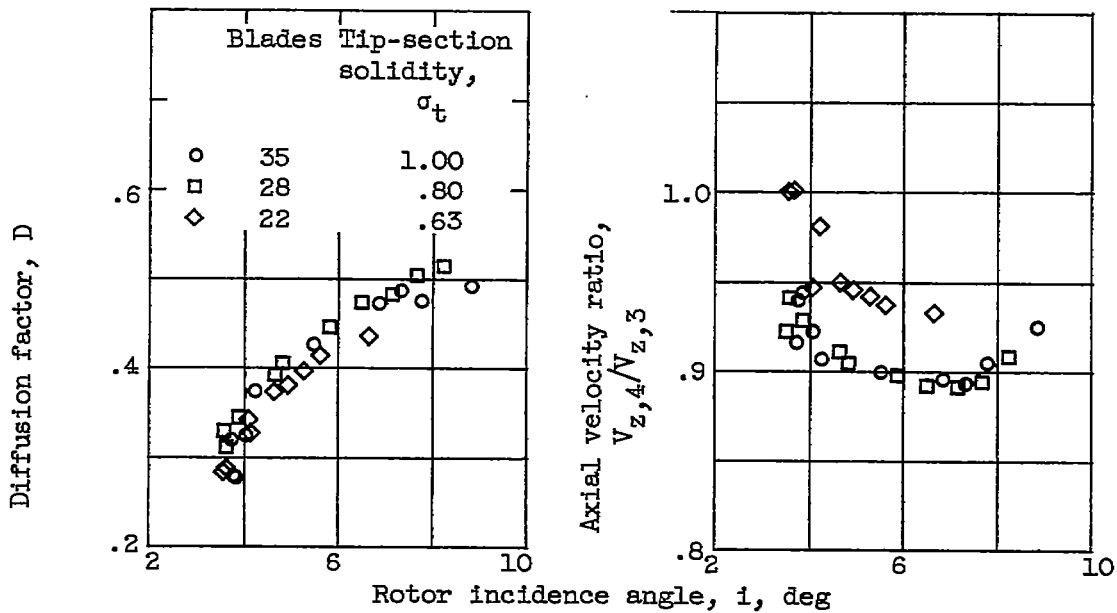
Figure 9. - Variations of diffusion factor and velocity ratio
with incidence angle for three solidity levels of 1.5-inch-
chord transonic compressor rotor at tip section at design
speed.
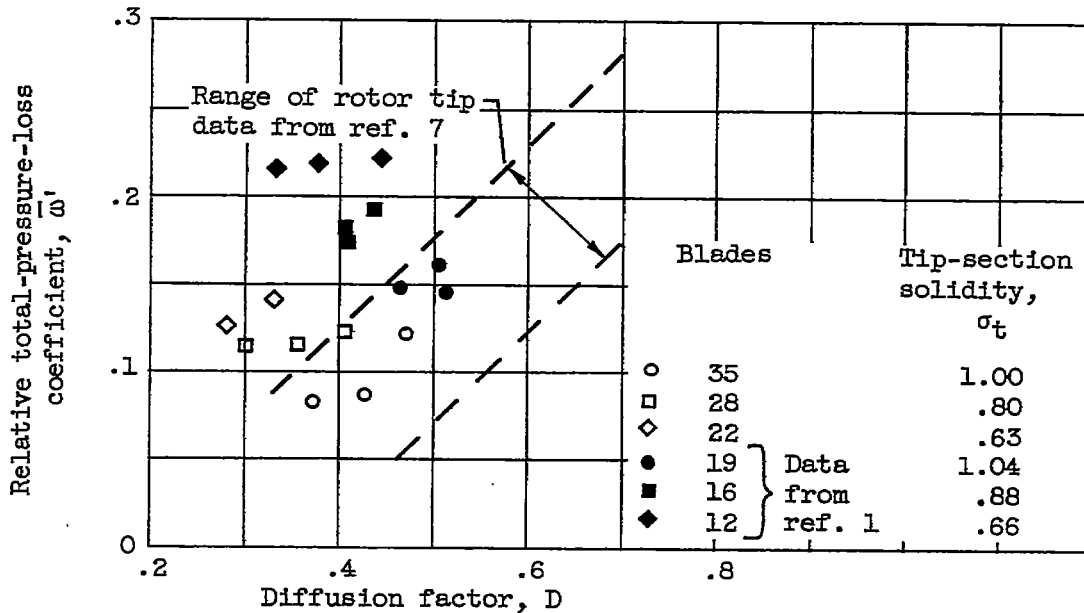
Figure 10. - Variation of tip-section relative total-pressure-
loss coefficient near minimum loss with diffusion factor at
design speed for three solidity levels.

(a) 35-Blade rotor. Blade-element   (b) 22-Blade rotor. Blade-element
     solidity, 1.00.   solidity, 0.63.
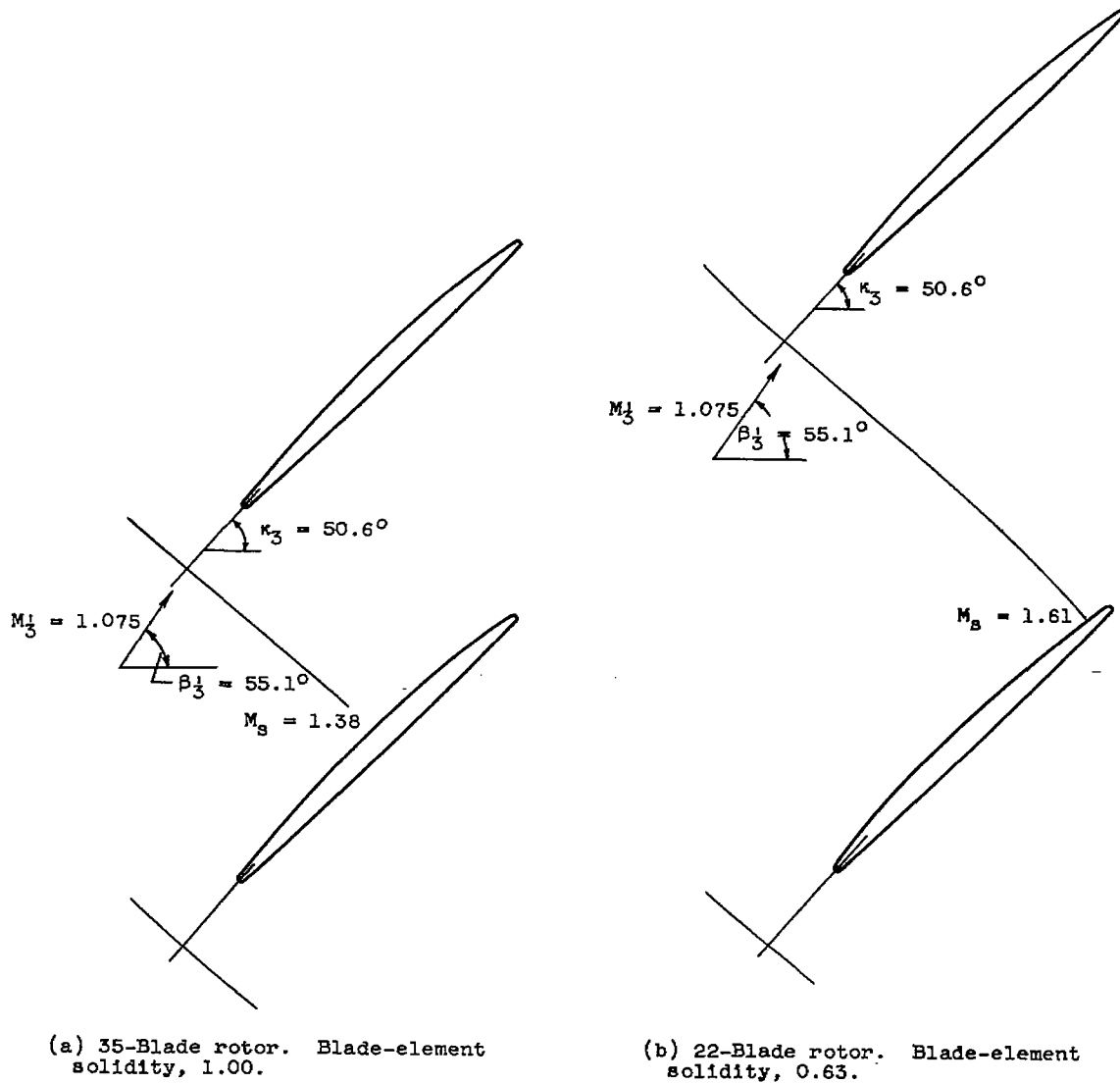
Figure 11. - Supersonic flow through a cascade indicating change with solidity of loca-
tion of bow wave on blade suction surface and resulting blade suction-surface Mach
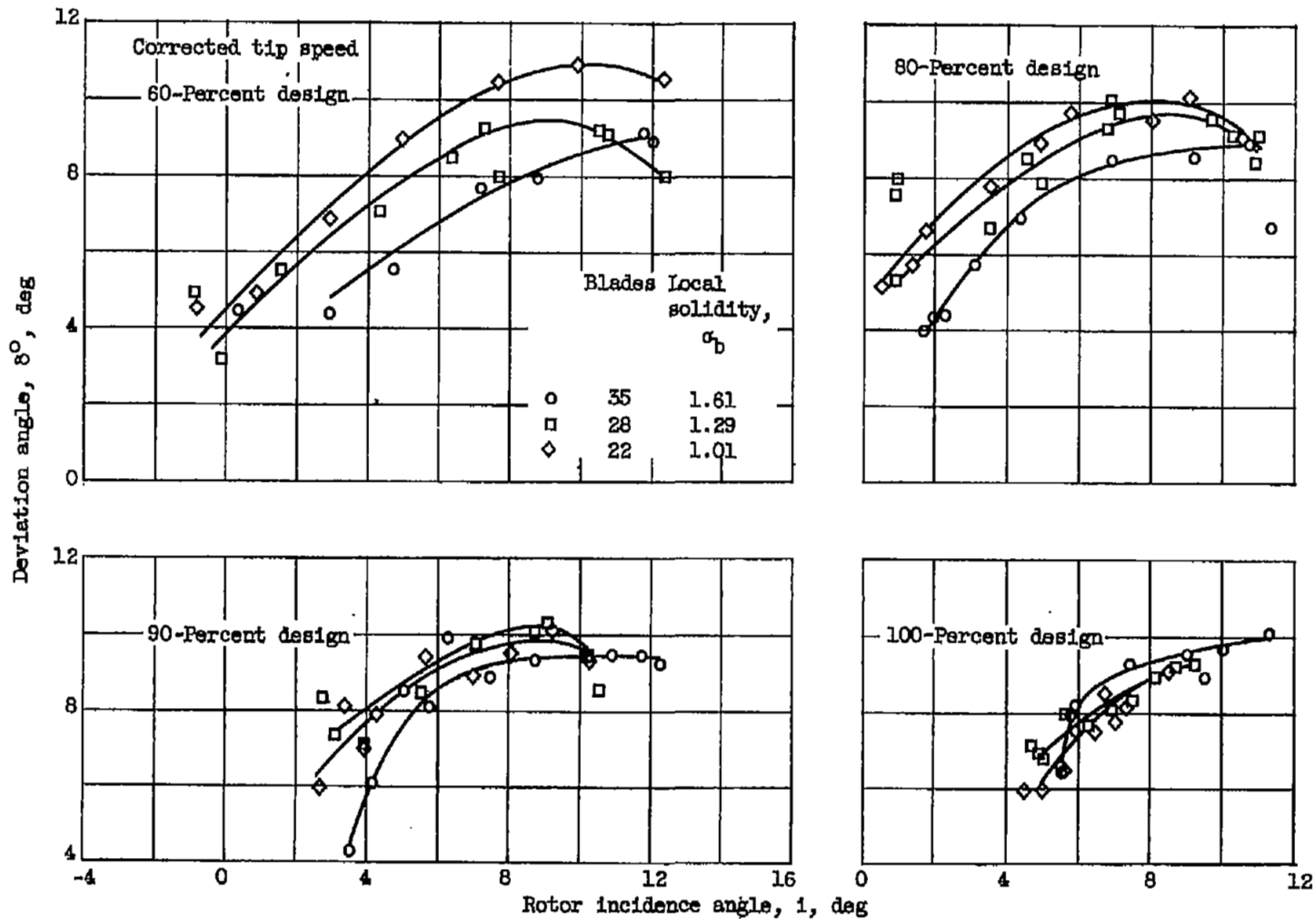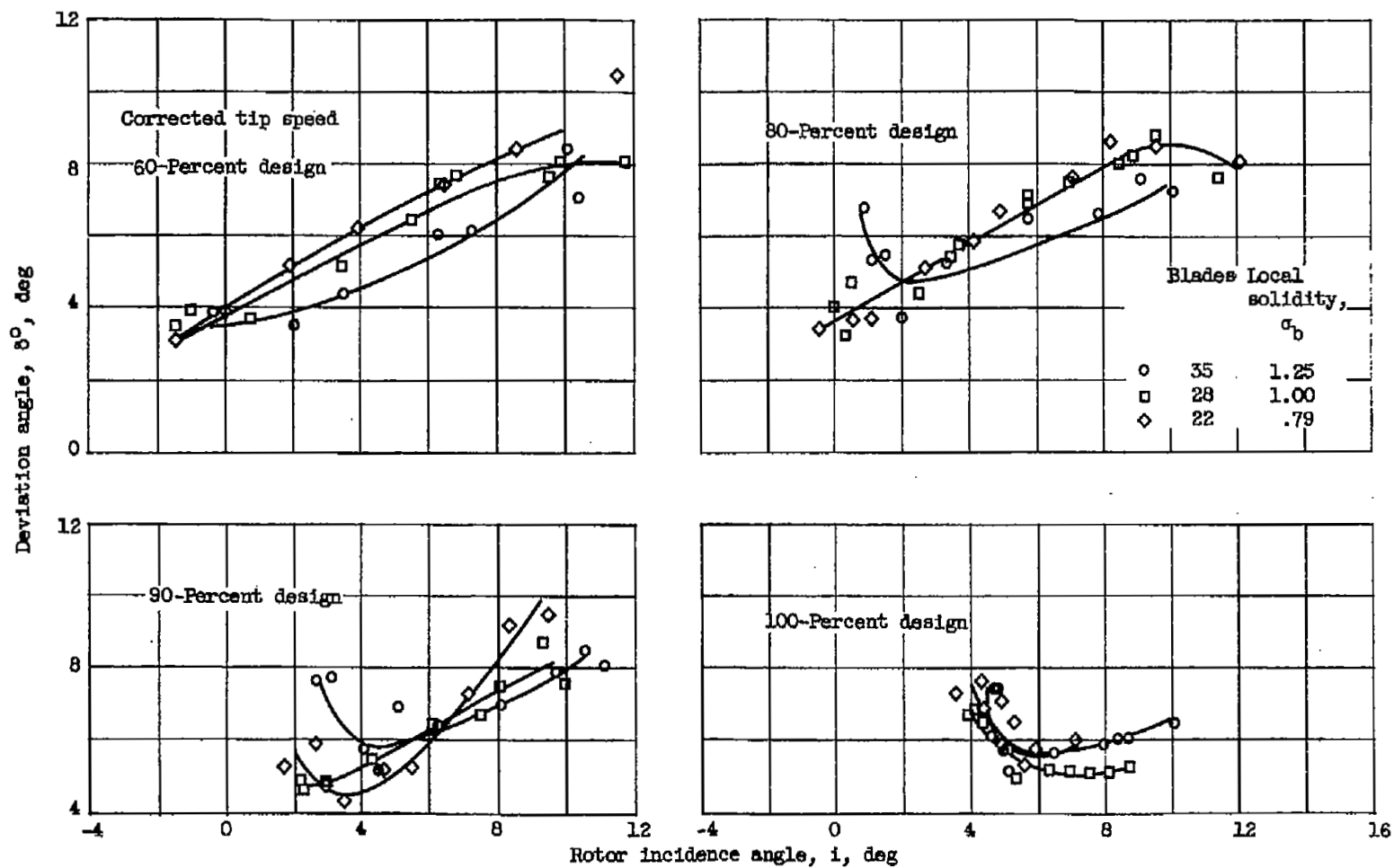numbers preceding the shock. Outlet radius, 8.60 inches.

(a) Hub section (r_4 = 5.64 in.).

Figure 12. - Comparison of deviation-angle variation with incidence angle for three solidity levels of 1.5-inch-chord transonic compressor rotor.

(b) Mean section (r_4 = 7.00 in.).

Figure 12. - Continued. Comparison of deviation-angle variation with incidence angle for three solidity levels for 1.5-inch-chord transonic compressor rotor.
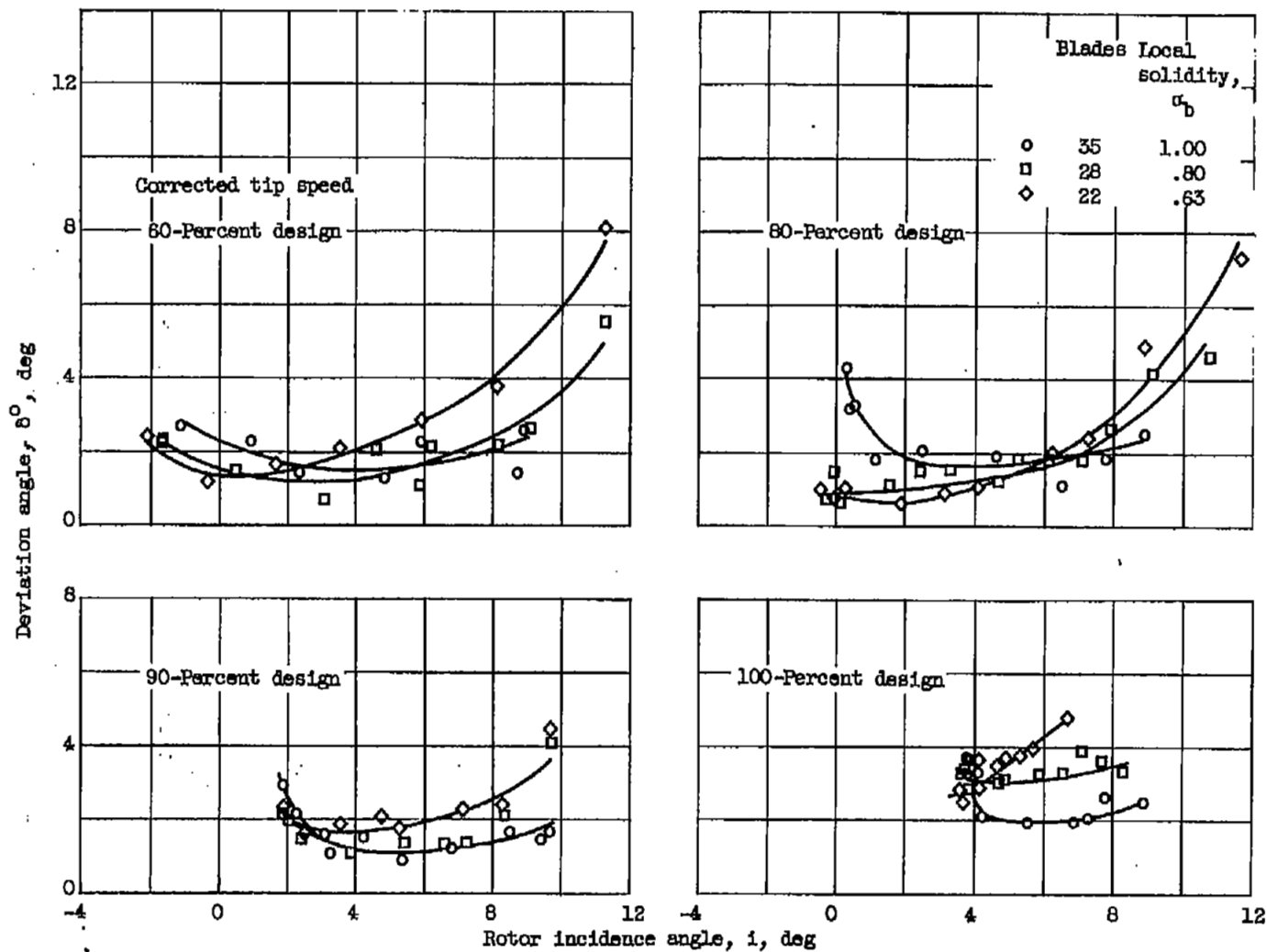
(c) Tip section (r_4 = 8.60 in.).

Figure 12. - Concluded. Comparison of deviation-angle variation with incidence angle for three solidity levels of 1.5-inch-chord transonic compressor rotor.
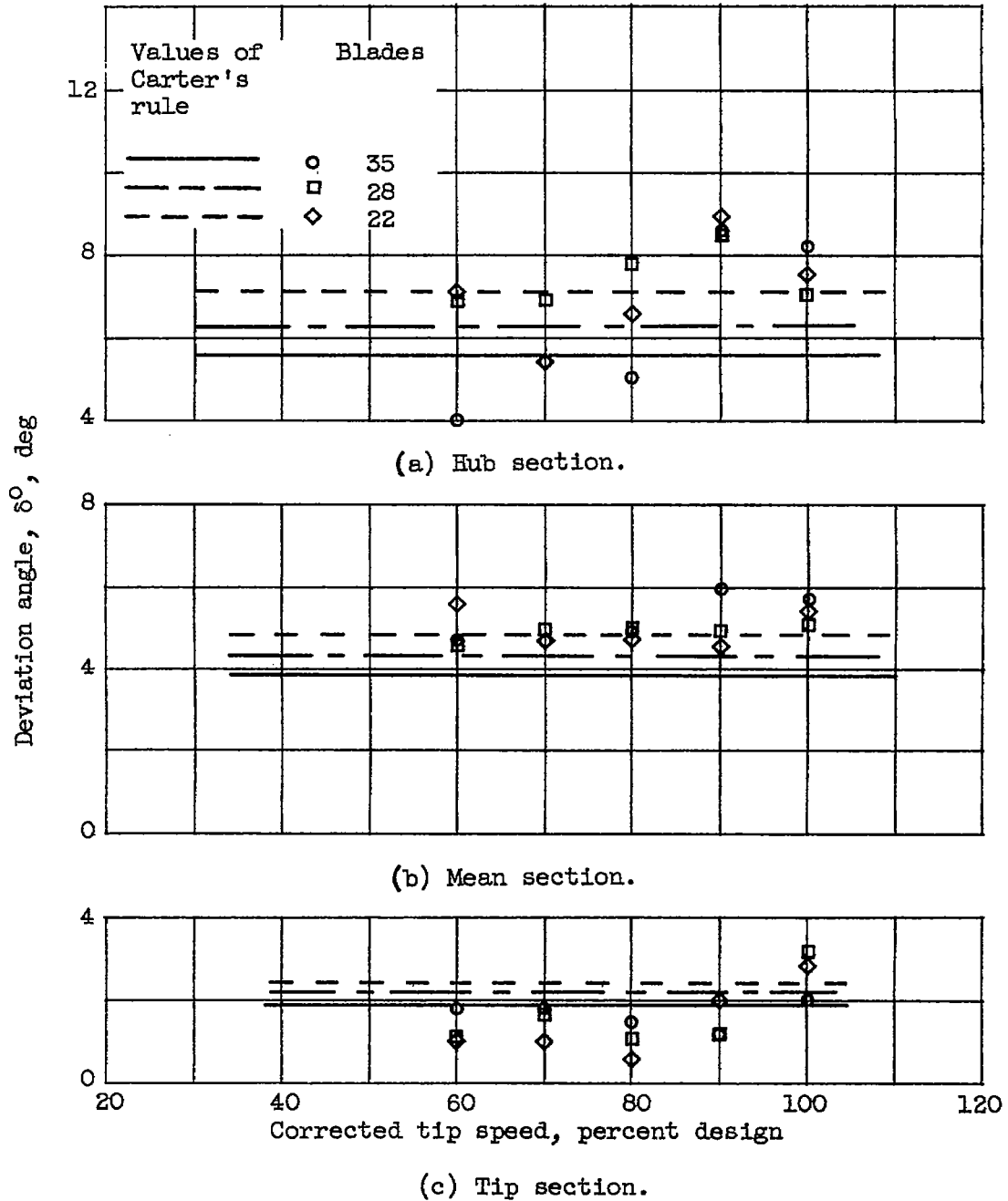
(a) Hub section.

(b) Mean section.

(c) Tip section.

Figure 13. - Deviation angles at minimum-loss incidence angle for three solidity levels of 1.5-inch-chord transonic compressor rotor.